Using Very-Low-Frequency Electromagnetics (VLF-EM) for geophysical exploration at the Albertine Graben, Uganda - A new CAD approach for 3D data blending

David Eggert

Dissertations in Geology at Lund University,
Master's thesis, no 579
(45 hp/ECTS credits)

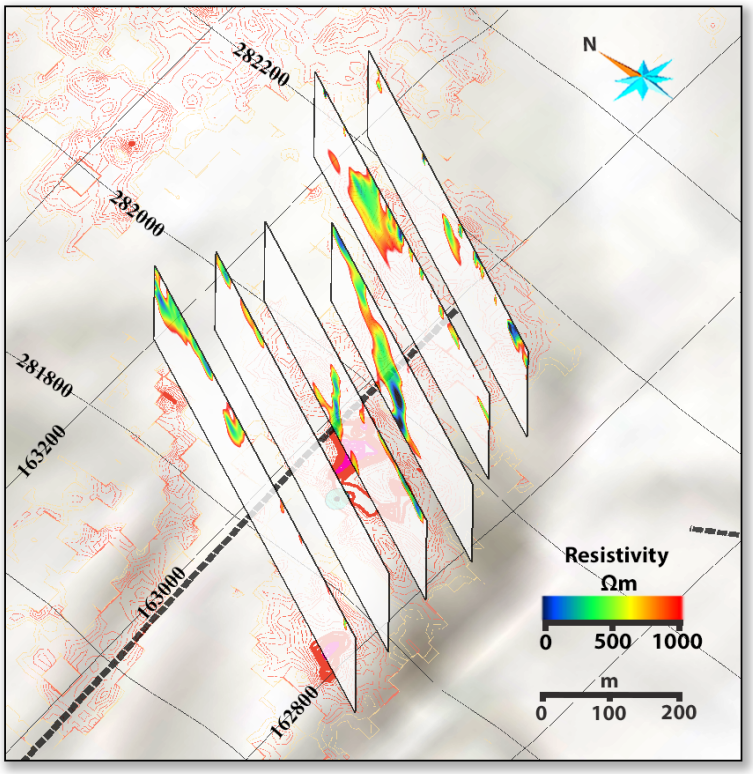

Department of Geology
Lund University
2019

Using Very-Low-Frequency Electromagnetics (VLF-EM) for geophysical exploration at the Albertine Graben, Uganda - A new CAD approach for 3D data blending

Master's thesis

David Eggert

Department of Geology
Lund University

2019

Contents

1 Introduction **7**
2 Regional geology and study area **7**
3 Methodology **9**
3.1 Very-Low-Frequency Elecetromagnetics (VLF-EM) technique
3.2 VLF-EM surveying
3.2.1 Acquisition and field work
3.2.2 Preparation and filtering
3.2.3 Inversion and visualization
3.3 Additional blending data
3.3.1 Remote sensing imagery
3.3.2 Geochemical analysis
4 Results **13**
4.1 VLF-EM results of Region 1
4.2 VLF-EM results of Region 2
5 Discussion **16**
5.1 VLF-EM survey dependencies
5.1.1 Time
5.1.2 Direction
5.1.3 Locality
5.1.4 Anomaly
5.2 VLF-EM results analysis
5.2.1 Anomalies in Region 1
5.2.2 Anomalies in Region 2
5.3 VLF-EM results blended with additional data
5.3.1 Multiple analysis Region 1
5.3.2 Multiple analysis Region 2
6 Conclusion & summary **21**
7 Acknowledgements **23**
8 References **24**
APPENDIX I
APPENDIX II

Cover Picture: Example of one VLF-EM frequency result blended with iron anomaly map from remote sensing satellite data in 3D space and additional DEM basemap in grayscale and geological fault as dashed line.

Using Very-Low-Frequency Electromagnetics (VLF-EM) for geophysical exploration at Albertine Graben, Uganda - A new CAD approach for 3D data blending

DAVID EGGERT

Eggert, D., 2019: Using Very-Low-Frequency Electromagnetics (VLF-EM) for geophysical exploration at Albertine Graben, Uganda - A new CAD approach for 3D data blending. *Dissertations in Geology at Lund University*, No. 579, 28 pp. (45 ECTS credits) .

Abstract: Electromagnetic waves, also known as radio waves, which propagate at low frequencies of only 3 kHz to 30 kHz, are usually used for communication with submarines. However, these waves can also be used on land to measure differences in the electrical conductivity of the subsurface. This technique is called Very-Low-Frequency Electromagnetics (VLF-EM) and has been successfully used to gain an insight into the geological properties of the subsurface.

In the present work, these VLF-EM measurements were performed in an active rift valley in Uganda, East-Africa (Albertine graben) to locate suspected anomalies in the form of ore deposits. The data were processed and displayed in a three-dimensional space and thus made it possible to visualize distinctive areas. To validate these striking areas, additional geological data such as remote sensing and geochemical rock analysis and geological maps were blended with VLF-EM results in 3D space. Thereby promising zones could be found, which indicate anomalies by different data. The VLF-EM methodology has proven to be quite cost effective compared to other geophysical exploration methods, but it does harbor a number of peculiarities that should be considered in advance.

Keywords: Albertine Graben, EAR, East-African-Rift, Exploration, Geology, Geophysics, Ore, Uganda, Very Low Frequency, VLF-EM

Supervisors: Ulf Söderlund (Lunds universitet), Rouwen Lehné (Technische Universität Darmstadt)

Subject: Bedrock Geology

David Eggert, Department of Geology, Lund University, Sölvegatan 12, SE-223 62 Lund, Sweden. E-mail: davideggert@mailbox.org

Användning av Very-Low-Frequency Electromagnetics (VLF-EM) för geofysiska undersökningar i Albertine Graben, Uganda - En ny CAD-strategi för 3D-datainsamling

DAVID EGGERT

Eggert, D., 2019: Användning av Very-Low-Frequency Electromagnetics (VLF-EM) för geofysiska undersökningar i Albertine Graben, Uganda - En ny CAD-strategi för 3D-datainsamling. *Examensarbeten i geologi vid Lunds universitet*, Nr. 579, 28 sid. 45 hp.

Sammanfattning: Elektromagnetiska vågor, även kända som radiovågor, är vågor som sprider sig med låga frekvenser från 3 till 30 kHz. Dessa lågfrekventa vågor används vanligtvis när man önskar kommunicera med ubåtar. De kan emellertid också användas på land för att mäta skillnader i jord– och bergarters elektriska konduktivitet. Denna mätteknik kallas Very-Low-Frequency Electromagnetics (VLF-EM) och har framgångsrikt använts för att få en inblick i underlagets geologiska egenskaper.

I detta projektarbete utfördes VLF-EM-mätningar i en aktiv riftdal (Albertine graben) i Uganda i Afrika för att lokalisera misstänkta avvikelser i form av järnrika malmer. Datan bearbetades och visas i ett antal tredimensionella sektioner för att åskådliggöra potentiellt intressanta zoner. För att validera dessa kompletterades VLF-EM datan med annnan geologisk information, såsom fjärranalys och geokemisk bergartsanalys. Därmed kunde potentiellt intressanta zoner hittas, identifierade såsom anomoalier. VLF-EM-metodiken har visat sig vara en kostnadseffektiv metod jämfört med andra geofysiska undersökningsmetoder.

Nyckelord: Albertine Graben, EAR, East-African-Rift, Geofysik, Geologi, Malm, Uganda, Utforskande, Very Low Frequency, VLF-EM

Handledare: Ulf Söderlund (Lunds universitet), Rouwen Lehné (Technische Universität Darmstadt)

Ämnesinriktning: Berggrundsgeologi

David Eggert, Geologiska institutionen, Lunds Universitet, Sölvegatan 12, 223 62 Lund, Sverige. E-post: davideggert@mailbox.org

1 Introduction

Electromagnetic (EM) radio waves in the very-low-frequency (VLF) range are the major tool for communication of submarines. In the 1960s this method was first modified for geological investigations in Sweden by Paál (1965), and is still in use, even if it includes decisive restrictions for reception and processing. However, the efficiency of ever more advanced computers and algorithms opened up new opportunities for VLF surveys. Thus, this study is intended to apply the VLF-EM method for investigating a potentially highly ore-rich area in the Albertine Graben in Uganda, East-Africa (Figure1).

Uganda has an area of over 240 000 km² with a population of about 33.6 million. Its climate is warm and tropical, with temperatures up to 30°C. Between March and May and between September and November are the rainy seasons in Uganda, in which VLF-EM investigations are not to be recommended due to the electronic measuring instruments and the an unfavorable alteration of the electrical properties of the soil. Circa 180 km southwest of the western branch of the Kilembe area at the foot of the Ruwenzori Mountains (figure 1, top right), lies the largest copper mine in Uganda, where approximately 4 million tons of copper and undefined amounts of incidental cobalt are suspected (Owuor 2019). According to the Ministry of Energy and Mineral Development Uganda (2018), approximately 50 million tonnes of iron ore are estimated in the Kabale area (also in southwestern extensions of the western branch rifts) in southwestern Uganda. Additionally, petrolum reserves have been discovered in the Albertine Graben (AmanigaRuhanga & Manyindo 2010).

This work is based on the assumption that certain anomalies in form of ore grade rocks exist in the investigated area which should be narrowed down locally with the help of this work. In the course of the previous investigations regarding the collaborations of the Geological Survey of Uganda, the Darmstadt University of Technology, Gernany and the company Rockinol Limited, the studied area was selected for the VLF-EM surveys Therefore, these two main objectives of this study should be achieved:

- Identification of underground (max. 200 m depth) anomalies in form of ore grade rocks in several profiles using VLF-EM measurements with subsequent data inversion of the measured profiles.
- Blending obtained data with additional geological data within a georeferenced 3D model to locate potential anomaly locations as a basis for future reconnaissance drilling.

Therefore, the proposed M.Sc. project overlaps with previously mentioned research by the Darmstadt University of Technology, Uganda Geological Survey and the company Rockinol Ltd., which holds the license for the study area and funds the research. Previous investigations of the cooperation include field work on site with rock analyses, remote sensing to map superficial peculiarities and geomagnetic investigations, which, however, in the area of the study area was not sufficiently resolved.

In this context, indicators for anomalies were found by remote sensing analysis and field campaigns in which existing rocks have been geochemically investigated. This research will be considered in this thesis and will be blended and discussed in combination with the newly surveyed VLF-EM data from 2019. As indicated by the results in certain places, outstanding zones have been localized. It turned out that certain findings coincide giving increased indications of particular areas.

2 Regional geology and study area

The study area is located within a classical rift system called East-African-Rift (EAR). This rift, which extends over several thousand kilometers across Africa, widens progressively with up to 5 cm/year (Kampunzu *et al*. 1998). Between the major African Nubian plate continent and the African Somalian plate drifting towards southwest, the lithosphere is opening to form an early stage of an oceanic basin (Simiyu & Keller 1997). Due to the diverging plate boundaries of the African Plate with the Mid-Atlantic Ridge in the west and the Carlsberg Ridge in the east, the African Plate is actually under compression (Richardson 1992). The reason for extensional tectonics in East-Africa after Chorowicz (2005) derives from the Afar mantle plume of about 1000 km in diameter. The plume appeared 30 million years ago in Ethiopia and progressively thins out the lithosphere due to its enormous thermal energy causing doming in its center. Consequently, after Zoback (1992) the force exerted by enhanced buoyancy of the upper mantle against the force of the compression must be greater and thus contributes to the extension and thinning within the African continent. According to Morley (1989), the crustal thickness in the western branch is only about 15 to 30 km, while Prodehl *et al*. (1997) have identified a general crustal thickness in eastern Africa of 40 ± 5 km. The brittle continental crust subsequently fractured, forming normal faults and graben or half-graben. Progressive thermal uplift of the whole rift results in scarps and graben shoulders, which are subject to erosion and fill off the interstitial basins with sediments.

The EAR can be further divided into two different branches, which have also developed individually (figure 1). The western branch runs from North Uganda arched over 2500 km to Mozambique and includes Lake Albert (Mobutu), where the study area is in close proximity. Shoulders of these rift zones are several kilometers wide and its average western shoulders are generally more elevated than the eastern shoulders. The characteristic tectonics of the western branch displays a half-graben with lengths between 80 to 160 km and 30 to 60 km width (Rosendahl 1987). The origin of the western branch, however, is not as clearly as the

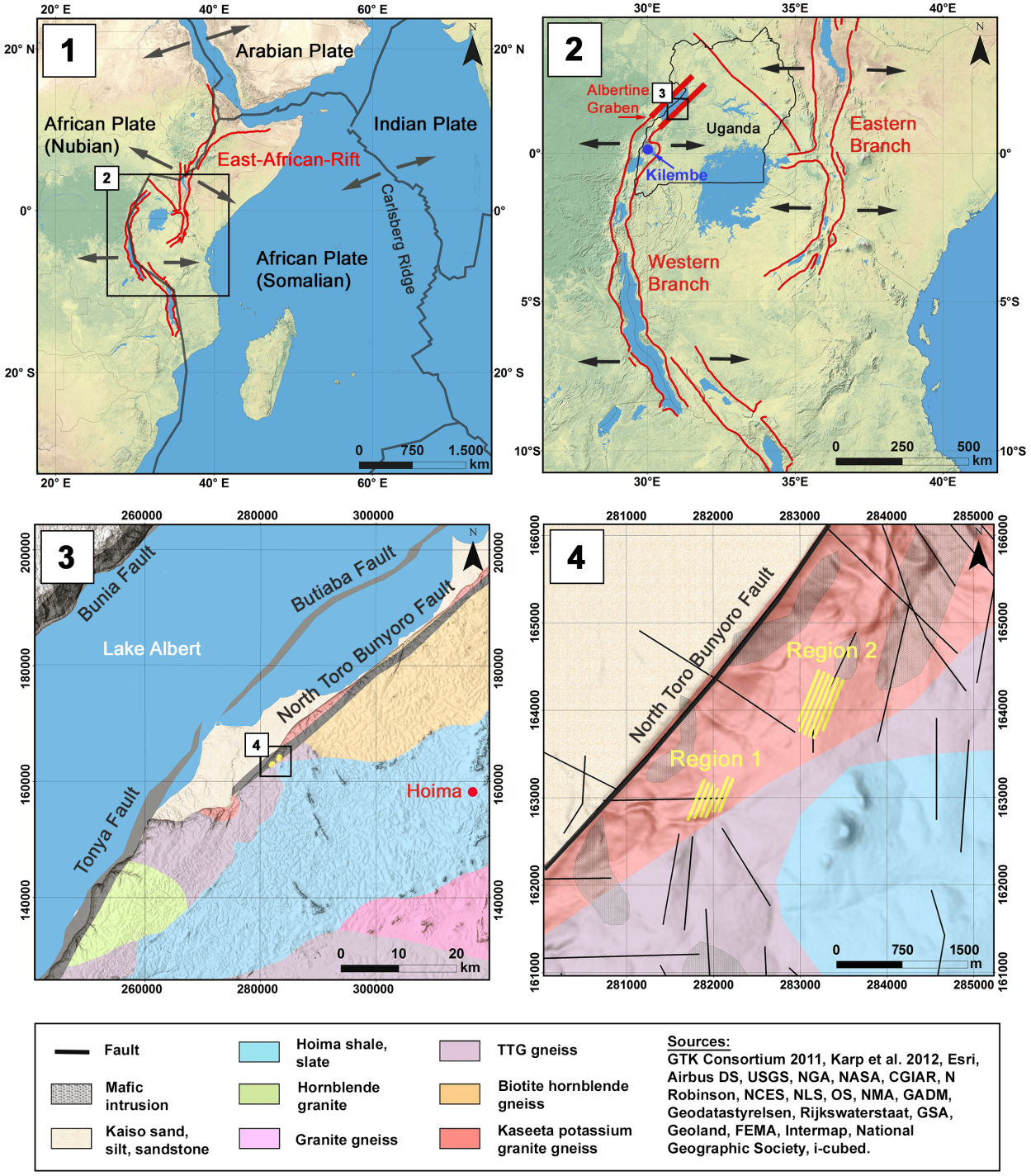

Fig. 1. Overview map of East Africa with the East African Rift (EAR) and the different tectonic plate boundaries and directions of movement (1). The EAR is further divided into a western and eastern branch (2). In the north of the Western branch in Uganda lies the northernmost rift called Albertine Graben. There, the main faults (North Toro Bunyoro and Tonya fault) run equally Northeast to Southwest direction (3). In immediate proximity to the North Toro Bunyoro fault on the rift shoulder at ca. 1100 m above sea level the study area is situated. In this area, two different regions (1 and 2) were investigated. The direction of the yellow profiles was determined by the consistent response from the Australian VLF transmitter NWC during the first VLF signal receiving test to obtain the best possible resolution. Explanations on the relationship between profile direction and VLF transmitter are discussed in 5.1.(4).

development of the entire rift in East Africa. According to Ebinger (1989) and Upcott *et al*. (1996) it originates pure extensional dynamics that lead to tectonic horst-and-graben structures and normal faults, which also appear to be representative of the whole EAR. Especially Morley (1989) considers that compression in the western branch must have occurred in addition to sheer extension. However, Abeinomugisha & Kasande (2013) have worked out essential propositions for additional compressional regime during the formation of the western branch in the Albertine Graben.

The Albertine Graben itself describes the northernmost basin of the western arm with a length of about 500 km and a width of about 50 km, beginning at the northern border of Uganda with Sudan up to the end of Lake Edward. The lakes Albert, George and Edward are located from north to south within the Albertine Graben. The Lake Albert is ca. 130 km long and ca. 35 km wide with a maximum water depth of 58 m and comprises the northernmost lake of the western branch of the East African Rift. Overall, the rift in the Lake Albert area yields a symmetrical graben structure with the Bunia fault in the Northeast and the Tonya or North Toro Bunyoro fault in the Southeast (figure 1). In contrast other rifts in the western branch, show asymmetric characteristics. The Bunia fault strikes between 40°N and 60°E and the North Toro Bunyoro fault on the eastern side of the graben runs from 40°N to 60°E, forming a 90 km long escarpment which exceeds Lake Albert by more than 400 m in the east (Upcott *et al*. 1996). In southeastern continuation the Tonya fault strikes from 20°N to 35°E approx. 85 km, also causes an escarpment of several hundred meters. At the transition between the North Toro Bunyoro fault and the Tonya fault, which is located approximately in the middle of the east coast of Lake Albert, a complex zone formed which is interpreted as a relay ramp. In addition, the Butiaba fault lays at the northeastern connection to this ramp, which dips at only 40° and forms a littoral platform at the east coast of the lake (Karp *et al*. 2012). Exactly where the North Toro Bunyoro Fault and the Tonya Fault converge and presumably form that relay ramp lies the investigated area of this study. This study area is therefore located approximately 8 km east of Lake Albert and ca. 35 km to the west of the city of Hoima in northeastern Uganda (figure 1). It is ca. 2 km² in size, topographically comprising a ridge (the eastern Albertine graben shoulder) that descends steeply from 1200 m a.s.l. (meters above sea level) to 800 m a.s.l. towards the lake.

The regional geology in the study area is thus strongly linked to the evolution of Lake Albert's graben formation and will be considered chronologically subsequently. Although it is generally agreed that the aforementioned graben structures are appearances due to the extension of the crust, there are also structures within the rift that indicate compression. Accordingly, the direction of expansion or compression of the crust in the Lake Albert area is the subject of a considerable amount of research and does not always yield a uniform derivation of the rift evolution of the Lake Albert area. The initial rifting in the Lake Albert area at Albertine Graben began in the late Oligocene (~25 Ma) to Early Miocene (~20 Ma). In the Mid Miocene (~12 Ma) compression occurred while rifting again reoccurred in the Pliocene (~4 Ma) followed by another period of compression during the Pleistocene (~2 Ma) (Delvaux & Barth 2010). At Lake Albert, the rift is active and shows an extension in northeast-southwest direction, as well as in east-west direction (Nyblade & Langston 1995). Strecker *et al*. (1990) also show that the direction of extension has rotated gradually over time. Additionally, Abeinomugisha & Kasande (2013) argue that this regime of alternating compression to extension has led to complex fault zones that facilitated the trapping of vast hydrocarbon deposits within the Lake Albert rift.

Regarding the geological development on a large scale of the EAR and also on a smaller scale of the study area at Lake Albert, the following is noticeable: The rift processes, whether de-compressional or compressional, are geologically so young with a few tens of millions of years that they could be described as recent. If, however, one observes studies of the exposed rocks, their enormous age differences stand out. In the study area and in the large area of eastern Lake Albert, rocks from the Neoarchaean with more than 2500 Ma aging can be found. Particularly in the investigated area this is predominantly Kaseeta potassium granite gneiss with an approximate age of 2732 ± 8 Ma but also quartzite and schist (figure 1) with occasionally appearing mafic intrusions. About 200 meters southeast of the study area runs the boundary to the slightly younger Tonalite-Trondhjemite-granodiorite gneiss (TTG gneiss) rock formation, which also originates from the Neoarchaean. That boundary is readily exposed, which means it is not covered and runs approximately parallel to the main North Toro Bunyoro fault direction from southwest to northeast (GTK CONSORTIUM 2011).

3 Methodology

3.1 Very Low Frequency Electromagnetics (VLF-EM) technique

Very-Low-Frequency-Electromagnetic (VLF-EM) is a technique that utilizes electromagnetic waves in the Very Low Frequency range to determine conductivity variations in the subsurface. This "Very-Low-Frequency" comprises the frequency range from 3 Kilohertz (kHz) to 30 kHz in the spectrum of electromagnetic waves (figure 2). The corresponding wavelengths range from 100 km (frequency 3 kHz) to 10 km (frequency 30 kHz). A primary signal is emitted by the antennas primarily used to communicate with submarines. This primary signals produce secondary signals induced by bodies with high electrical conductivity in the subsurface (McNeill & Labson 1991).

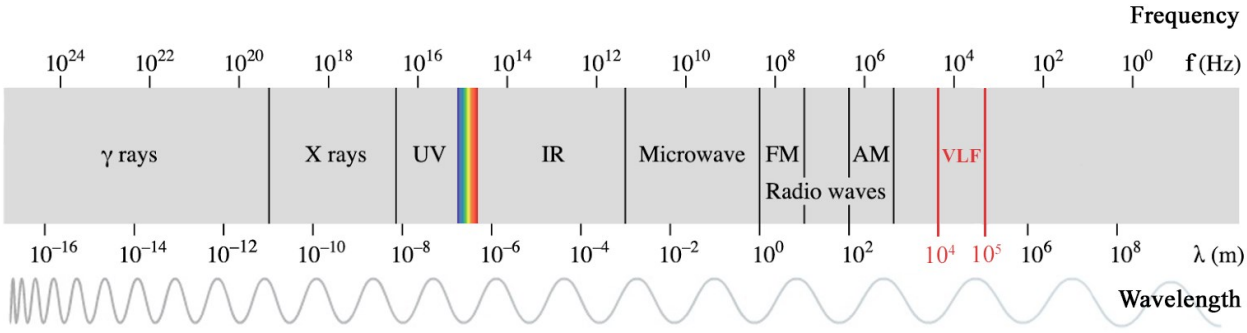

Fig. 2. Very-Low-Frequency (VLF) is in the range of long-wave radio waves in the electromagnetic spectrum with frequencies from 3 kHz to 30 kHz. The corresponding wavelengths range from 100 km to 10 km. The wavelengths are increasing from left to right, while the frequencies are decreasing. Between Ultraviolet (UV) and Infrared (IR) the colored visible light spectrum is situated (created after Verhoeven (2017)).

The following section describes how geological insights can be obtained from this VLF signal for submarine communication and is based on the work by Knödel (2005) and Reynolds (2011). The underlying physical electromagnetic principle is explained in Appendix I and a more in-depth explanation of the technical VLF-EM parameter handling is given in Appendix II.

Electromagnetic waves (occasionally called radio waves) are emitted by the VLF transmitting antenna. As the name implies, these waves have 2 components, a magnetic and an electrical which in the conduct of this work will be regarded separately and referred to as fields. The VLF-EM is based on the analysis of the magnetic field component, which propagates horizontally from the transmitting antenna (figure 3). At the area to be investigated, this primary signal can of course be measured with the VLF device, but the essential factor is the secondary signal, which is not horizontal, but vertical. This secondary vertical signal of the magnetic field is only generated if there are electrically conductive sources in the subsurface of the study area (Pedersen *et al*. 2009). Hence, a measured vertical magnetic component in the VLF frequency range is inevitably an anomaly, since this vertical component needs to be induced first (Knödel 2005).

A parameter frequently mentioned in the context of VLF-EM measurements is the tilt angle, which simply describes the relation between the primary and secondary magnetic field. This angle, in turn, indicates to which extent the primary magnetic field is impinged by the secondary magnetic field. The magnetic field lines of the secondary induced field span to a certain extent circles whose side directly above the body runs parallel to the surface and thus the angle of the resulting field changes signs by crossing an anomaly horizontally at the surface (figure 4). Accordingly, if a profile is measured over an electrically conductive body, the tilt angle is first positive, then zero, and after that negative. As shown in figure 4, the point at which the tilt angle equals zero is called the crossover point and indicates the position of the conductive body in the underground.

In summary, an electrically conductive body generates a vertical secondary magnetic field by electromagnetic induction from the horizontal primary magnetic field of the transmitted VLF signal. Through the combination of the horizontal and induced vertical components, the resulting magnetic field is created, which is measured on the surface by the VLF-EM device. The relation between strength and direction of the secondary magnetic field to the resulting total magnetic field provides then insight into the location of electrically conductive areas in the subsurface (Monteiro Santos *et al*. 2006).

3.2 VLF-EM surveying

3.2.1 Acquisition and field work

Three different frequencies were utilized with its corresponding transmitters located on several continents (see Table 1 and figure 5). Two different areas were defined within the study area, which are here referred to as region 1 and region 2 (figure 1). The

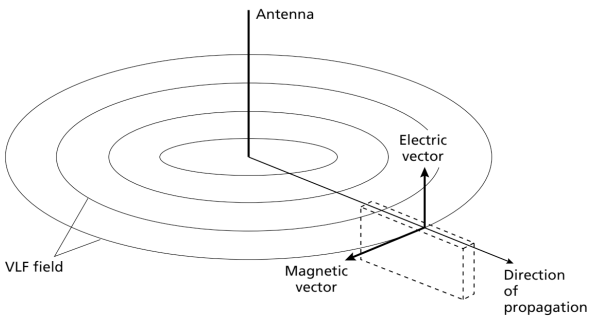

Fig. 3. Schematic illustration of the primary VLF field with the components of the magnetic and electric field. The electric field propagates vertically while the magnetic field is perpendicular and therefore horizontally. Both components are perpendicular to the direction of propagation from the transmitting antenna. Dashed lines show a suspected anomaly in the subsurface which extends in propagation direction (figure by Kearey *et al*. (2001)).

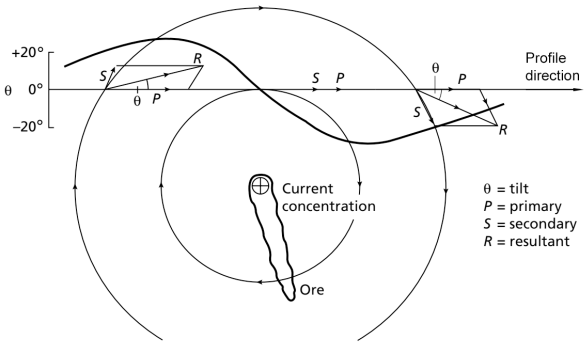

Fig 4. Schematic illustration of the primary, secondary and resulting signals of the magnetic field. This figure shows a cross section through the study area of an entire profile with a suspected ore body in the subsurface. While the primary magnetic field (P) is horizontally aligned, a secondary magnetic field (s) is induced by the ore body and vertically inclined. Both fields repel each other to form a resulting field (R). These variables change in strength (shown here as length of vectors) and in phase shift (shown here as tilt angle) while a measurement is made along the profile. Since the magnetic field lines are concentric around the ore body, the fulcrum of the curve (bold black curve) indicates the approximate center of the body. How these transfer variables are processed in detail is explained in Appendix II. (figure by Kearey *et al*. (2001)).

profiles in region 1 are in the southwestern part of the study area and have lengths of ca. 450 m and a vertical penetration of ca. 160 m. The profiles of region 2 located in the northeastern part of the study area, have an average length of ca. 700 m and a penetration of ca. 160 m. These regions are considered as two separate study areas as they are about 1 km apart. Mentioned coordinates and all figures are referenced to the Universal Transverse Mercator (UTM) 36N on basis of the World Geodetic System 1984 (WGS84).

Measurements in the field took place from 08.02.19 to 12.02.19 and were acquired using a GEM GSM-19V VLF device. Profiles with the 500 to 800 meters length in NE- SW direction were defined using a differential GPS. A distance of 10 meters was defined between the individual measuring points on these profiles, the distance between the individual profiles was 60 meters. The GEM GSM-19V VLF device includes a measurement console, a GPS receiver and a VLF device, which can be carried by one person. First, a transmitter search was started to find up to the maximum number of 3 transmitters with a sufficient signal strength. The measurement started at the first profile point, where the device was kept stable and parallel to the earth's surface. Each individual measurement was stationary and thus not performed during movement. If the measurement was successful after 5 to 15 seconds, the acquired value was displayed directly. If the instrument was at an unfavorable measuring angle, the measurement was stopped and the direction in which the instrument should to be rotated was displayed (for deviations of 10° from the horizontal plane). In this way, a new measurement was recorded every 10 meters until the defined end of the profile. Then, the measurement was directly switched to the adjacent profile and carried out in the opposite direction on this profile. It took about 30 to 40 minutes to perform the measurement of one individual profile.

3.2.2 Preparation and filtering

The recorded data was loaded as a .txt file from the GEM GSM-19V VLF device. In addition to the VLF-EM values in phase and out of phase, the GPS coordinates, time, altitude (topography) and of course the frequency and signal strength of the transmitter were recorded for each single measurement. It is necessary to process the VLF-EM raw data through a series of geostatistical algorithms to create understandable visualizations from the difficult to conceive VLF-EM values for in-phase and out-of-phase. In the past, this has been a major constraint, since filtering the data itself has been very time-consuming. In the progress of digitalization, computer-aided methods have been developed for this purpose. In this study the software VLF2Dmf by EMTOMO® was used. This program is adapted to read data from the GEM GSM-19V VLF device, to filter the data according to established algorithms, to invert and to interpolate the data.
In the following, the applied procedure will be described chronologically.

1. Import of the raw data from the .txt file generated by the GEM GSM-19V VLF device.
2. Application of a three-points moving average filter to obtain a smooth-running curve of the measured values.
3. Application of the Fraser filter (Fraser 1969). This filter algorithm is a four-point weight average fil-

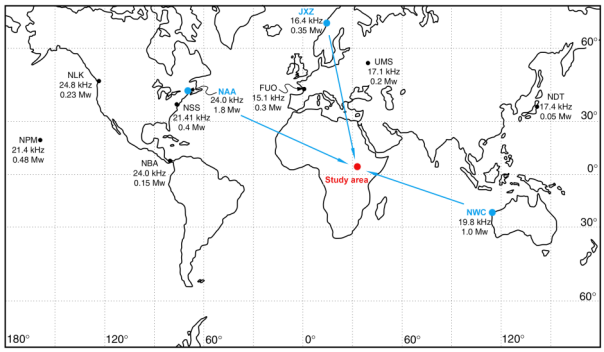

Fig. 5. Location of the main transmitters in the VLF range on the global map. The transmitters used for this work are shown with their respective incidence direction to the study area. These include the Norwegian transmitter JXN in Gildeskål, the US-American transmitter NAA in Cutler and the Australian transmitter NWC in North West Cape. It is important that the arrows are only a schematic indication of the direction, as the earth's curvature must be considered at these distances. (figure by Reynolds (2011), edited)

ter for converting noisy non-contourable data into less noisy contourable data and making the different ranges of measurement points consistent. It also generates peaks at the turning points of the measured values and thus indicates areas of increased conductivity. Intermediate values are created by adding and subtracting the measured values at certain points. For example, if the intermediate value between measuring points 2 and 3 is to be determined, it is calculated by the following formula. f2,3 = (M3 + M4) - (M1 + M2).

4. Application of the Karous-Hjelt filter (Karous & Hjelt 1983). This filter is a further development of the Fraser filter, which takes 6 measuring points into account for calculation. It uses the in-phase part of the VLF-EM data to create pseudo-sections with the same current distribution that would result from the measured magnetic field. VLF2Dmf used Karous-Hjelt weights: 0.102, -0.059, 0.561, -0.561, 0.059, -0.102.
5. Application of the apparent resistivity filter. It is important to specify a realistic value for the resistivity of the subsurface, because this value cannot be calculated. Hence, it is beneficial to identify the bedrock or, at best, to use electrical methods to measure the conductivity (Basokur & Candansayar 2003). Due to the dry magmatic and metamorphic rocks with low sedimentary deposition, a resistivity of 2000 Ωm was assumed (according to resistivity data by Dentith & Mudge (2014)).

3.2.3 Inversion and visualization

The subsequent step emphasizes the generation of an initial model response. In this step it is possible to determine whether resistivities change in the subsurface, for example when sediments or known lithology changes are involved, and to adapt the model accordingly. Since this was not expected originally, a uniform model including topography was used. It is assumed for the model that the bedrock has a high electrical resistivity of ca. 103 - 105 Ωm, as is usually the case for crystalline igneous or metamorphic rocks (Dentith & Mudge 2014) for the following data inversion according to Sasaki (1989). This algorithm generates a 2D model consisting of numerous rectangular blocks, where each block has a constant resistivity. The used configuration was damping factor 3.0, damping decreasing factor 0.9, iterations 15, data error for real and imaginary 0.02, since these parameters are recommended for a highly resistive subsurface above 1000 Ω m in the VLF2Dmf manual by EMTOMO®.

Previously, only 2D models were created for each profile. Since there are 6 profiles for one frequency, the next step is to load the data into a 3D program to view the appearance in context. Therefore, the inverted 2D model was exported as .png image file and as .xyz file for further importing into EMERSON® SKUA-GOCAD™. The obtained data from the program VLF2Dmf includes .xyz files and the associated .png image file. In principle, the .xyz file contains information on conductivity in three-dimensional space, i.e. the coordinates, depth and measured value for each profile. The .png image file reflect simply the areas of equal conductivity based on the data stored in the .xyz format. The visualization was achieved by two different procedures. First, the .xyz files from VLF2Dmf were used to create 2D interpolation profiles in SKUA-GOCAD™. The processing in SKUA-GOCAD™ had to be done to highlight areas with resistivities below 1000 Ωm or to make only areas with low conductivities visible. For this purpose, a cross-sectional surface was created from the .xyz files which corresponds to the profile line of the measurement and in which the measuring points lie. The coordinates and measured values were then projected onto this surface and its resistivity property was subsequently interpolated using the DSI algorithm (Mallet 1989).

3.3 Additional blending data

3.3.1 Remote sensing imagery

A further technique for blending VLF-EM data is geological remote sensing using satellite imagery. For this purpose, images are taken by the satellites Landsat and ASTER, which fall within the frequency range beyond visible light in the infrared range. By subsequent evaluation of the images, different colors of the visible light are simply assigned to these signals in order to investigate the different properties of the subsurface. Of course, this is not the actual color of the surface. This work requires profound knowledge of remote sensing and above all a lot of experience. For this reason, the processed data is kindly provided by Dr. Bert Rein. In principle, areas were highlighted in red color that indicate increased iron concentrations on the surface. The implication is that increased iron concent-

Table 1. Overview of the used transmitters in the VLF range with their key parameters (data from McNeill & Labson (1991)).

Name	Location	Frequency [kHz]	Power [kW]	Distance [km]	Direction
JXN	Gildeskål, Norway	16.4	350	~ 7400	NNW
NWC	North West Cape, Australia	19.8	1000	~ 9400	ESE
NAA	Cutler, Maine, USA	24.0	1800	~ 10500	NW

Table 2. Overview of the two regions in the study area with the frequencies used, the signal strength of the transmitter and the date of the measurement.

Region	Day	Signal strength [nT]	Frequency [kHz]	Transmitter
1	08.02.2019	~ 1 - 2	19.8	NWC (Australia)
	10.02.2019	~ 0.3 – 0.6	19.8	NWC (Australia)
			16.4	JXN (Norway)
			24.0	NAA (USA)
2	09.02.2019	~ 1 - 2	19.8	NWC (Australia)
			24.0	NAA (USA)
	11.02.2019	~ 0.6 – 0.8	16.4	JXN (Norway)
			24.0	NAA (USA)

rations may indicate rocks that also have high iron concentrations and occur and weather at the marked locations (Butz *et al*. 2018).

3.3.2 Geochemical analysis

In the context of that previous research in the study area in August 2017, the surrounding rocks were examined by Dr. Rouwen Lehné and Dr. Bert Rein in order to identify possible locations for further exploration. Samples of the rocks were taken and afterwards examined in the laboratory by Dr. Christoph Butz. The Bruker S1 Titan Model 800 was used to determine the element concentrations of these rocks by x-ray fluorescence (XRF). Of the 23 rock samples collected, 5 were considered for this work, which were found in the immediate vicinity of the VLF-EM measurements and explained in the context of the discussion under 5.3.

4 Results

The results of the VLF-EM surveys are presented in the following as 2D pseudo-sections. A pseudo-section describes the results of the VLF-EM measurements in vertical direction. Electrical resistivities are solely calculated based on the magnetic measurements and are not measured directly. The coloured profiles shown in Figures 6 and 7 therefore represent sections of the subsurface that are expected from the calculations and not direct measurement results of the electrical resistivity. The procedure for creating these profiles is explained as part of the methodology section.

The limits for the visualization of the anomalies were set to 1000 Ωm, as this is the best approach to reveal the structures. Below 500 Ωm can be considered as outstanding, as this value means less than half the regular value of the expected rock resistivity. Accordingly, high electrical resistivities are indicated in red and low electrical resistivities in blue. The interesting areas or also called anomalies are the blue areas, because low electrically resistive zones are being sought. The white areas within a profile display high electrical resistivities (more than 1000 Ωm) and are therefore in the red color spectrum. Only the junction at 1000 Ωm is shown in red here, but not the areas above 1000 Ωm, since the focus lies mainly on low electrical resistivity (blue). As described in the methodology under 3.2, the study area is divided into 2 regions and will be considered separately in the following. Table 2 provides an overview of the key data of each investigation.

4.1 VLF-EM results of Region 1

In region 1 six profiles were recorded on 08.02.19 with a frequency of 19,8 kHz. In profiles 4, 5 and 6 only the upper 30 m show enhanced conductivity, slightly increased up to approx. 50 m in the northeastern part of profile 5 at coordinates 281500/163200. In profiles 1, 2 and 3, on the other hand, a similar pattern can be seen. At the northeastern end of the profiles, conductive areas are already visible at the profile bottom, which run approximately by 45° in a southwesterly direction until they reach the upper edge of the profiles after 150 m. The conductive areas are also visible at the bottom of the profiles, which is most distinctly recognizable in profiles 2 and 3. Furthermore, anomalies can be detected in the continuation of the profile from approx. 200 m from the northeast, which dip from the upper 30 m of the profiles to almost the profile bottom towards the southwest.

The measurements from 10.02.2019 at 16,4 kHz resulted in a total of only 5 profiles, as the frequency in the first profile was not receivable at all. Areas of low conductivity are found halfway through profile 3 as spherical areas on the profile bottom. In continuation on profile 4, also slightly on the middle, there is also a rounded area of approx. 25 m diameter with low conductivity. Here, anomalies can still be identified at the top 10 m on half of the profile which were previously slightly smaller in profile 2. Anomalies are also recorded at the northeastern ends of profiles 5 and 6 near the surface (about 30 m), running about 200 m in southwestern direction.

The identical 6 profiles with the equal frequency of 19,8 kHz recorded 2 days later on 10.02.19

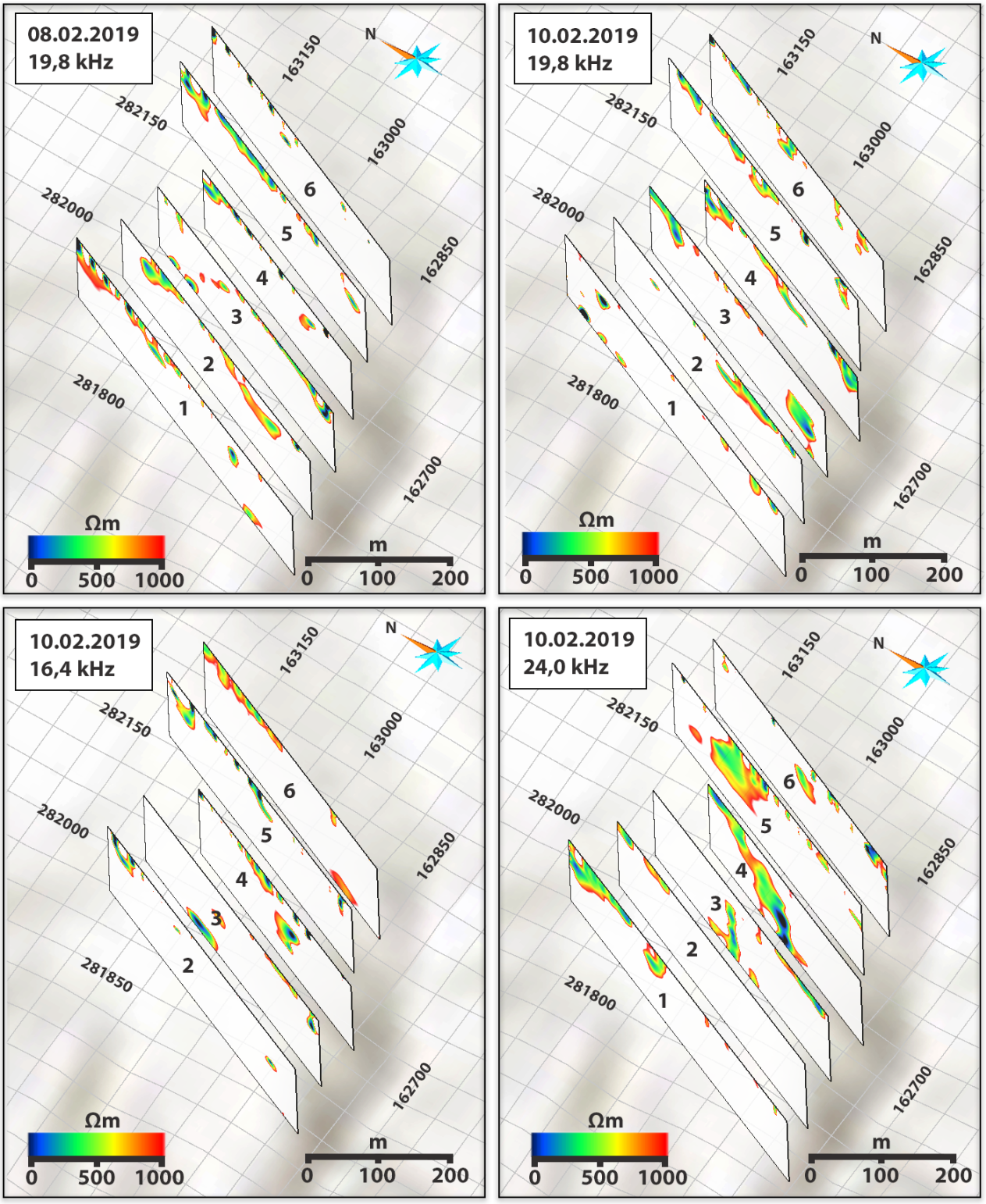

Fig. 6. The individual pseudo-sections of Region 1 are displayed as 2D profiles and resemble the VLF-EM results. Thereby the profiles are always at the same position but measured with different frequencies at different times (see box upper left corner). All profiles lie on a digital elevation model (DEM) of the surface of the terrain, which is displayed in gray scales. An UTM 36N grid with a length of 50 meters per cell is included. The colors in the profiles itself correspond to the expected electrical conductivity (according to the calculated model under 3.2.3).

show low conductivity at the southwest end of profiles 2, 3 and 4. While in profile 2 and 4 low conductivity up to approx. 30 m also occurs in the near-surface areas, in profile 3 these are in the lower area from 30 m to the bottom of the profile. In addition, at the northeastern beginning of Profile 1 there is an area of spherical anomalies in the order of 10 meter from the lower end of the profile to the upper end. Only shallow conductivity near surface areas can be found at the northeastern beginning of profiles 3, 4, 5 and 6. The characteristics of the anomaly in profile 3 at coordinates 282000/163130 are also visible in parallel extension towards east-northeast in profiles 4, 5 and 6.

The 6 profiles of 10.02.19 measured at a frequency of 24,0 kHz exhibit clear anomalies of low conductivity. Especially the profiles 3 and 4 show a band of approx. 30 m width from the surface to the bottom of the profiles. In profile 3 this band is almost vertical, in profile 4 it is 45° from the northeast to the middle of the profile. There are also striking areas in the first 50 m along profiles 1 and 2 from the northeast. The thickness here is a slightly greater of about 60 m in profile 2 and 30 m in profile 2. Profile 5 has a prominent area of low conductivity around point 282150/163100, but this is not seen in the following profile 6.

4.2 VLF-EM results of Region 2

In the following the 4 different measurements in region 2 are outlined. At the frequency of 19,8 kHz measured on 09.02.2019, distinct zones with relatively low conductivity below 1000 Ωm can be observed. Especially at the southwestern end of profiles 1, 2, 3 and 5 these areas are predominantly apparent at the surface but also up in depths of almost 100 m. The most prominent zone, however, is at the northeastern end of profiles 2, 3, 4 and 5, where extensive areas of low conductivity are visible from the surface to the vertical end of the profiles. Starting there from the northeastern end at the bottom of profiles 2 and 3, the area extends further southwest and forms an approximately 80 m wide zone that does not reach the surface. Instead, after approximately 250 m from the northeast, this zone becomes smaller and moves southwest only in the upper 30 m of both profiles 2 and 3. In profile 4, the extension of the low conductivity areas is confirmed and even extends from surface to ground at the northeastern beginning of the profile.

Measurements at 24,0 kHz on 09.02.2019 show the most distinct anomalies in profiles 1, 2, 3 and 4. The first profile exhibits low conductivity stripe of about 50 m at the southwest end at coordinates 2830500/1640500, which appears to be dipping from south west direction from the surface to the bottom of the profile. The anomalies in profiles 2 and 3 look approximately identical and show a spherical area of low conductivity of approximately 100 m in diameter at the bottom of the profiles at approximately 300 m from the northeast. This spherical shape tends to spread in diameter towards the bottom of the profiles. A similar large area is found at the northeastern end of profile 4, which does not extend all the way to the bottom of the profile but rather occupies only the upper half of the profile. This area appears the inverse, as its spherical shape is extended upwards and not downwards as in the case of the two profiles 2 and 3.

Extended areas of low conductivity in the measurements of 11.02.2019 at 16,4 kHz are clearly visible in the profiles 3 and 4. The anomaly extends from the bottom of profile 3 at the northeastern end to the surface of the profile diagonally falling approx. 200 m in southwestern direction. Profile 4 also shows an extensive zone of low conductivity at the northeastern end, which takes up the entire depth of the profile and, also extends to approx. 200 m in a southwesterly direction. In addition, anomalies can also be seen in profile 1 at the southwest end of the profile that begin approximately 50 meters below surface and extend to the end of the profile. In the subsequent profile only a small zone of low conductivity can be recognized at the bottom of the profile with a diameter of approx. 100 m and approximately in the middle of the entire profile. Other prominent areas appear in profile 5, starting at the surface at the extreme southwester end. From there this zone falls with approx. 45 ° in the northeast direction and reaches after approx. 200 m the bottom of the profile and forms a stripe of about 50 m width. The extended anomaly in profile 5 is not seen on adjacent profiles 4 and 6. In profile 6, only a 20 m wide strip appears on the surface at the outermost northeastern end for approximately 150 m.

In the profiles from 11.02.2019 at 24,0 kHz, the low conductivity areas are concentrated mainly in the southwestern area of profiles 2, 3, 4 and 6. Further areas are located in the northeastern part of profiles 1 and 5. Profile 1 shows an area of approximately 100 m depth from surface to the northeast. In a further extension in this profile, approx. in the middle, a narrow strip of approx. 20 m width can be seen which begins just 20 m below the surface and then ends again 20 m before the end of the profile. In the next profile 2, this strip can also be identified even if the strip is a slightly larger area approx. 20 m below the surface. In the southwestern area of profile 2 at coordinates 283100/164000, a large area of low conductivity extends from the surface to 20 m in front of the bottom of the profile. This area also extends to profile 3, even to the bottom of profile three. In the northeast of profile 3 there is a narrow zone of about 15 m at the bottom of the profile. This pattern is neither noticeable in profile 2 nor in the adjacent profile 4. The following profile 4 shows only one single area of low conductivity, that is, at the outermost south-western end. Here it seems as if a strip of about 50 m from the surface at the extreme southwest end to about 150 m in length extends to the bottom of the profile. A similar but much smaller area appears in profile 5 in extension. At the north-eastern end of profile 5, however, a strip of low conductivity of approximately 30 to two-thirds shows up in a south-westerly direction. This strip can-

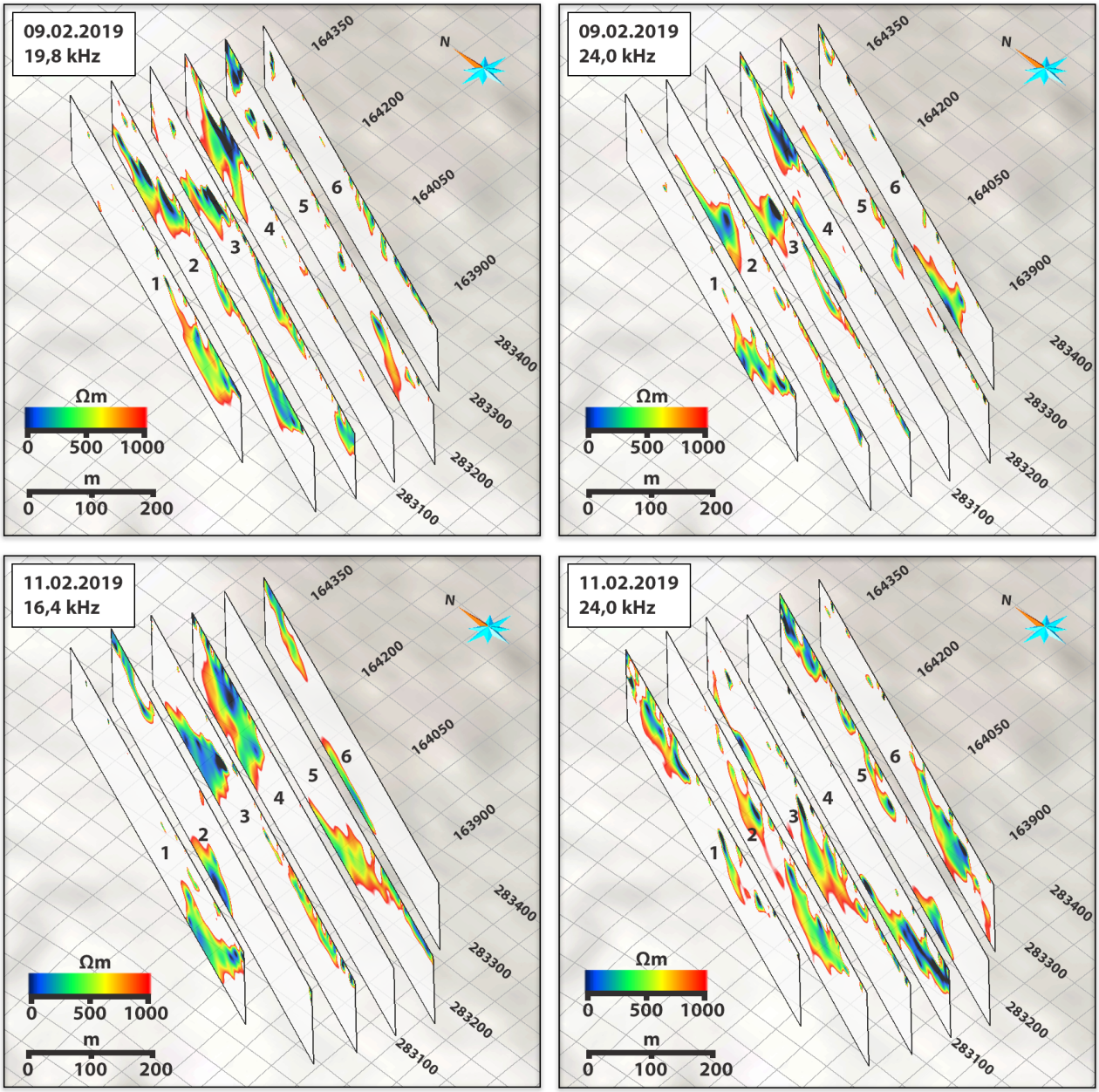

Fig. 7. The individual pseudo-sections of Region 2 are displayed as 2D profiles and resemble the VLF-EM results. Thereby the profiles are always at the same position but measured with different frequencies at different times (see box upper left corner). All profiles lie on a digital elevation model (DEM) of the surface of the terrain, which is displayed in gray scales. An UTM 36N grid with a length of 50 meters per cell is included. The colors in the profiles itself correspond to the expected electrical conductivity (according to the calculated model under 3.2.3).

not be seen in profile 4 or in profile 6. Only the outermost southwestern area of profile 6 shows an extended area of approximately 150 m length and 50 m width, which begins approx. 30 m below the surface and continues until close to the bottom of the profile.

5 Discussion

5.1 VLF survey dependencies

Even if the VLF-EM surveys can be carried out simply and quickly in comparison to other geophysical measurements (e.g. Geoelectrics), they still yield a variety of peculiarities that should be considered carefully to avoid errant interpretations. In addition, these characteristics also affect the results and the interpretation of the anomalies to different extents. For this reason, all factors are briefly explained in this paragraph and discussed in the following paragraphs based on the obtained data. The intention is to evaluate which factors have an influence on the VLF-EM results and, most importantly, how heavily weighted they are expected to ascribe and thus to evaluate how reliable the VLF-EM outcomes can be. Unless otherwise stated, the assertions mentioned are based on the very detailed explanations provided by McNeill & Labson (1991).

5.1.1 Time

The transmitter antennas have very distinct times during which no broadcasting is done at all due to maintenance schedules. However, these time intervals can be derived from the manual of the GEM GSM-19V VLF device manual in advance and therefore did not play a role in this work. Not only diurnally differences can be observed in the activity of solar radiation, but also seasonally and suddenly exceptional occurrences such as sunspots. The optimal time for the survey is from early morning to noon, because the electromagnetic disturbances of the ionosphere induced by the sun radiation are usually minimal then. VLF waves are reflected by the fee electrons in the ionosphere, which enables the transmission of these electromagnetic waves over thousands of kilometers in the first place. Furthermore, thunderstorms also generate so-called sferics, i.e. natural electromagnetic fields (Kearey *et al*. 2001). In case such a thunderstorm is located between the transmitter and the area under investigation, the output signal can be attenuated. Since these factors only influence the primary signal, but not the secondary signal induced by the suspected anomaly, it is sufficient to simply determine the strength of the primary signal. The used GEM GSM-19V VLF device can scan the signal and shows the signal strength of the transmitting antenna (refer table 2). The manufacturer's specifications in this regard are as follows: excellent results are expected from 5 Nanotesla (nT) upwards, useful measurements are still possible below 5 nT and below 0.5 nT indicates that the data is unusable (GEM Systems 2008).

5.1.2 Directions

The directional relationship between the expected anomaly and the transmitting antenna of the VLF signal is probably one of the most important of all. De facto, VLF-EM results always depend ultimately on how the expected anomaly is in aligned to the transmitting antenna. If the expected anomaly should be perpendicular to the direction of a used transmitted signal of the antenna, it is highly unlikely that any anomalies will be detected by measuring the magnetic field component. The reason for this is the electromagnetic induction, which is described in Appendix I. Briefly restated here, the area or volume to be flowed through is simply minimal if the expected body is directed perpendicular to the transmitting signal of the antenna. The device used for the work (GEM GSM-19V VLF) determines the magnetic field components, induced by conductivity differences in the subsurface. This method is called VLF-EM. However, there are also VLF devices, which additionally determine electric field components, which must be distinguished as VLF-R technique. In VLF-R, electrodes are placed in the ground to directly measure the electrical conductivity and to relate it to the magnetic field. This enables the detection of anomalies that are not aligned with the VLF transmitter but represents a considerable additional survey effort.

5.1.3 Locality

The composition of the subsurface at the survey site is of decisive importance. This applies in particular to the existing rock and the more impactful covering with soil, which is discussed after the country rock effects. The best conditions are found when the rock is as electrically resistant as possible, because the output signal is then barely attenuated and the conductivity contrast between rock and anomaly increases. The main variable that is very influential and is also used in other electromagnetic techniques is the skin depth. This value defines the investigation depth or indicates when the signal has already been attenuated to such an extent that signal beyond the skin depth can no longer be considered. The skin depth can be determined with the following formula (1), where ρ is the host rock's electrical resistivity and f is the frequency of the antenna used. In the case of an electrically very conductive host rock, the skin depth decreases considerably e.g. for the used frequency of 19,8 kHz, the skin depth is about 160 meters with a host rock resistivity of 2000 Ωm. If the host rock has a resistivity of only 500 Ωm, the skin depth decreases by half down to 80 meters. This way also the maximum depths of the VLF-EM profiles or pseudo sections were determined, which were included in the results.

$$\delta = 500\left(\frac{\rho}{f}\right)^{\frac{1}{2}} \qquad (1)$$

The area investigated for this work consists to a large extent of crystalline metamorphic rocks such as gneiss and quartzite, occasionally mafic intrusions also occur. With electrical resistances in the order of 2000 Ωm for the surrounding host rocks and 100 Ωm for anomalies in form of mineralized rocks (values based on Dentith & Mudge (2014)),, good initial conditions can be seen. In general, crystalline rocks are optimal for VLF-EM measurements due to their high electrical resistances from host rock (Saydam 1981).

Accordingly, the covering of the existing rock also has an impact on the VLF-EM results. Since in most cases this covering consists of weathered rocks and soil, the effect is much greater than that of hosts rocks alone. The reason is that weathered material has significantly higher electrical conductivities and can even obscure underground anomalies. In this context, the term "overburden effect" is used, which refers to the extent to which the superimposed layers can affect the results. McNeill & Labson (1991) discovered that with a vertical contact between a medium of 10000 Ωm and one of 1000 Ωm and a covering of a medium of 100 Ωm with a thickness of 10 m, the results were reduced by about 30%. For this purpose, the thickness and the electrical properties are usually determined in order to incorporate them into the later model. However, in the investigated area no electrical measurements have been made. On the one hand, no equipment was available for this purpose, on the other

hand, the investigation area lies on a graben shoulder, as already described in the geological introduction. This leads to the material being eroded preferentially into the graben, in this case into Lake Albert, and these ridges exhibit only slight sediment cover.

To ensure a more detailed investigation it would be advisable to drill small boreholes in order to determine the sediment cover at different locations and to carry out subsequent geoelectrical measurements to determine the conductivities. These values should then be included in the model for inversion of the data. Despite this missing information, numerous spots of exposed bedrock at the studied area, it is assumed that the sediment cover might be considerably low. Drillings in the quarry development about 3 km south of the study area are further evidence for this. One borehole directly encountered existing bedrock, the second one encountered about 60 cm of sediment cover (Isabirye 2008).

The topography of the area to be investigated is likewise influential. Since different skin depths can be achieved by the topography, the effect cannot simply be calculated based on elevation data. Even if the study area is located on an elevated shoulder of the trench, the measured profiles are too short in relation to show significant height differences. The profiles are therefore neither located in topographical valleys nor on particularly high peaks.

5.1.4 Anomaly

Another significant aspect is the influence on VLF-EM results based on the properties of the expected anomaly in the study area. It should be noted that the measured signal induced by a possible anomaly is proportional to the contrast of the different conductivities and thus more important than the actual conductivity. Assuming there lies a fault in the subsurface with a conductivity of 100 Ωm in a host rock with 1000 Ωm. In case the fault would have a conductivity of 1000 Ωm and the host rock 10.000 Ωm the measured signal would be identical. In practice, it is rather unlikely that anomalies run exactly in a certain direction or have completely vertical angles. In the case that the anomalies lie vertically in the subsurface, no significant influences were detected even at 45° deviation from the vertical. This means that anomalies such as faults do not depend on the incidence angle but mainly on the contrast of the conductivity itself. Lastly, there is one question that arises frequently from the use of VLF-EM surveys and is directly related to the anomaly itself: Is it possible to determine through VLF-EM exactly which anomaly is present in the subsurface or, more precisely, to differentiate between a geological feature (e.g. fault) and an ore body? McNeill & Labson (1991) have therefore calculated the saturations of the signal based on the work of Saydam (1981) and Saydam (1984, unpublished). In other words, they determined the resolution with which the VLF-EM results are recorded and how exactly this can be attributed to the source and concluded literally: "[...] VLF measurements are generally poor for distinguishing between even moderately conductive geological structures and much more conductive ore bodies [...]". As a result, the following discussion refers to anomalies, i.e. areas in which high electrical conductivity can be assumed.

5.2 VLF-EM result analysis

5.2.1 Anomalies in Region 1

The outstanding feature of region 1 is that the 3 measurements at 19,8 kHz (both days) and 16,4 kHz only show smaller VLF-EM anomalies with a maximum diameter of 50 meters and solely the results at 24,0 kHz (10.02.2019) exhibit anomalies with a diameter of more than 100 meters (figure 6). Moreover, it is noticeable that the 24,0 kHz results do not show a consistent trend in the contiguous neighboring profiles. As soon as a larger anomaly occurs, which is more than 100 meters in diameter, as in profile 5, there is no longer any indication of this in profile 6. Even if profiles 3 and 4 resemble each other with an almost vertical anomaly, neither profile 2 nor profile 5 shows a similar shape. Since the profiles are indeed 60 m horizontally apart from each other, local low conductivities could occur between 2 profiles and not be present outside. For vertical dimensions of more than 100 meters displayed in these profiles, this assumption is rather unlikely. The signal strength of all frequency on 10.02.2019 varied between only 0.5 nT and 1 nT, which, according to the manufacturer, are critical measurement conditions (GEM Systems 2008). For this reason, the VLF-EM results of 08.02.2019 should have a significantly higher reliability than the results of 10.02.2019. Conversely, this means that it would be more reliable to consider the measurement on 08.02.2019 at 19,8 kHz and to use the reference measurement on 10.02.2019 at the same frequency as a comparison material, since this is where the fewest parameters for deviation are existing. Surprisingly, the results for 19,8 kHz on different days show almost no significant differences. Only superficial sporadic conductivity differences can be observed in both cases. Figure 6 shows that the initial signal originates at 19,8 kHz from the ESE direction (Australia). Accordingly, at this frequency all potential anomalies are optimally detected which are also in an alignment with this direction (refer explanation at 5.1.2). Similarly, at 24,0 kHz, only the signal originates from the opposite direction (USA). Therefore, the profiles at 19,8 kHz and 24,0 kHz are approximately at right angles to the original signal, which means optimum measurement coverage.

In contrast, at 16,4 kHz the transmitter is not at right angles to the measured profiles, but at approximately 30°. Thus, anomalies are amplified in NNW direction, i.e. roughly in the direction of the profile. This makes it more difficult to detect a tendency from neighboring profiles, since the suspected anomalies appear preferentially in profile lines or more precisely.

Anomalies that lie in the juxtaposition of the profiles can barely be determined in this frequency direction.

In conclusion, there is a striking area at the coordinates 281950/163000, though only the measurement of one frequency (24,0 kHz) provides distinct pattern, and the measurement at 16,4 kHz can slightly support this anomalous pattern by slightly similar pattern at profile 3 and profile 4. Due to the limited evidence by only one frequency VLF-EM result and the fact that more reliable data at 19,8 kHz exhibit no anomalous appearance, this area could yield high conductive material but needs further investigations in detail.

5.2.2 Anomalies in Region 2

The two different measurements at 19,8 kHz and 24,0 kHz both captured on 09.02.2019 in region 2 are very consistent in their appearance (figure 7). An extensive anomaly is appearing in the northeast of profiles 2, 3, 4 and 5, suggesting that the anomaly might increase in volume at depth. It is the largest area that has been confirmed by multiple measurements throughout the study. For example, the results on a different day and with a different frequency (11.02.2019 at 16,4 kHz) in profiles 3 and 4 show the largest anomalies of the entire campaign at this location. There, almost the entire profile thickness is occupied by areas of very low conductivity. In this context, the direction to the transmitting antennas of the respective frequencies should be considered. At 19,8 kHz and 24,0 kHz, the profiles are close to the transmitter at right angles and ensure good coverage of the investigated area. If an anomaly e.g. a fault runs in the direction of the transmitters, the output signal simplified said has the largest attack area and the secondary signal can be determined therefore very well. The measuring profiles are then placed perpendicular to the transmitter direction to ensure the best coverage. This can best be described using the example of a fault. If several profiles are placed in the direction of the fault, the entire extent of the fault will be shown in one profile. However, if the profiles are placed at a right angle to the fault, the fault will most probably be shown in all profiles at a certain position. Since the transmitter at 16,4 kHz is slightly in line with the direction of the profile (or shows an oblique angle of 30°), it can be concluded that the large conspicuous areas of low conductivity in profiles 3 and 4 are also present in this direction. Thus 3 different measurements from 3 directions point to the same zone in the study area. In addition, the measurements at 24,0 kHz are inherently inconsistent with many small areas and long anomalies, such as a patched rug and larger anomalies of a profile are not confirmed in surrounding profiles. Though it is theoretically possible, as in the description of region 1, that the anomalies are locally limited, i.e. smaller than the 60 m profile distance between each other, but if a conspicuous area is stretched several tens of meters or even more than 100 m in profile direction, the vertical orientation might be comparable or at least visible to certain degree. Furthermore, the input signal strength was more than 2 nT during the measurements of 09.02.2019 and the signal strength on 11.02.2019 with less than 1 nT. Hence, as similar for the previous mentioned results in region 1, the VLF-EM results of 09.02.2019 should have a significantly higher reliability than the results of 11.02.2019.

In summary, this area within a radius of 100 m around the coordinates 283250/164300 should be targeted for future investigations, as it shows conspicuous features by 3 VLF-EM measurements. In addition, these 3 measurements also indicate anomalies in the immediate vicinity of the coordinates 283100/164050. The results at 24,0 kHz on 11.02.2019 should be treated with caution because the anomalies cannot be confirmed by other VLF-EM measurements and the received signal strength was very low. The measurements at 16,4 kHz should also be viewed critically, even if some parts of the profiles with profiles from 09.02.2019 have similarities. The possibility for a coincidental match is of course also given.

5.3 VLF-EM results blended with additional data

5.3.1 Multiple analysis of Region 1

Since tectonic movements have occurred in this study area and the main fault is only a few kilometers away, it is quite conceivable that much smaller faults can arise in the vicinity. As shown in figure 8 and 9, an already mapped fault runs directly vertically from west to east. This fault hits profiles 3 and 4 directly where the previously described approximately vertical anomalies are located. The measurements on the same day (10.02.2019) at 16,4 kHz also show anomalies extending from the profile bottom to the surface, even if they are not as concisely vertical as at 24,0 kHz. However, the fault in all other profiles lies at about half the length and not only in profiles 3 and 4. Measurements at other frequencies do not show any signs of irregularities. Thus, results at 19,8 kHz (both days) and 16,4 kHz are quite consistent in the profiles 4, 5 and 6 with the surface elongated area of low conductivity and quite contrary to the measurements at 24,0 kHz. In addition, the overall areas of the anomalies are quite small, appear rather exclusively near the surface and otherwise sporadically, rather patchy.

In the overview map of figure 8, the concentrations of iron are obtained through remote sensing data from satellites. Superficial concentrations of iron naturally occur where rocks with ferrous minerals occur or are weathered. Since iron-rich source rocks also possess high electrical conductivity and low electrical resistivity, enhanced superficial iron anomalies indicate such subsurface rocks. As can be noticed in the study area, within and nearby region 1 and region 2, that enrichments with increased iron concentrations are recorded from remote sensing data. The prominent elongated area at coordinates 283200/162700 near the mountain is situated on a road that runs from southwest to northeast. An increased occurrence of

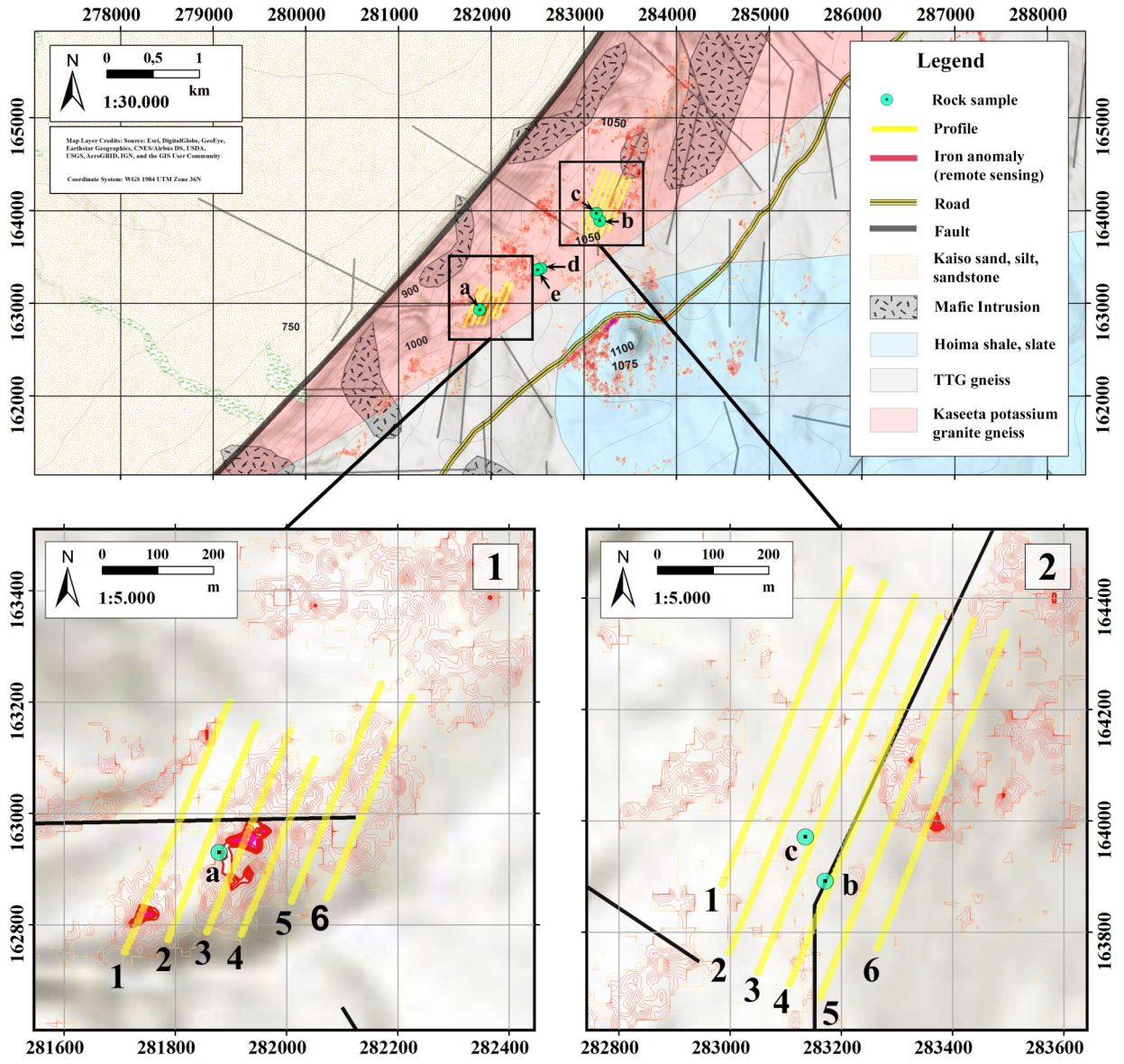

Fig. 8. The upper figure illustrates the regional geology of the investigated area in combination with remote sensing data. The lower two figures are enlargements of the different regions of the study area. Region 1 is shown at the bottom left, while region 2 is shown at the bottom right. The yellow lines are the respective profiles of the VLF-EM measurement in the corresponding plan view.

superficial iron anomalies is evident in region 1 compared to the vicinity of the profiles from this region. The highest anomalies are found at the southwestern beginning of profile 1, approximately 50 m in diameter in size, and most importantly at half of profile 3. At profile 3, the anomaly exhibits an extension of more than 100 m in diameter, the location that should be considered in association with additional data. Region 2, on the other hand, shows only sporadically smaller areas of anomalies in the 10 meters range. Only half of profiles 5 and 6 contain a zone with about 50 m diameter of increased iron concentrations. This area should therefore serve as a basis for consideration with other data.

An interesting location has been identified at coordinates 281900/162950, coinciding with the previously discussed VLF-EM anomalies in profiles 3 and 4 at 16,4 kHz and 24,0 kHz. Thus, the use of remote iron anomalies could be seen as a further indicator of this area if there were not another area of increased iron concentration at the direct southwest beginning of the first profile. The rock sample “a” identified as hematite ore in region 1 (figure 8) highly supports the observations of iron concentrations in the vicinity of profile 3. Hematite ore of course indicates that there are high concentrations of iron in the vicinity. These results also support the results of the VLF-EM measurements of 10.02.2019 at 24,0 kHz. Taken together there are VLF-EM anomalies, a fault, enhanced iron concentrations by remote sensing and a rock specimen. Regardless of these parallels, there can no protruding anomaly be found at other frequencies of VLF-EM measurements.

5.3.1 Multiple analysis of Region 2

In Region 2, a striking mapped fault (see figure 8 and 10) runs almost parallel to the profile direction on profile 4, which coincides with the appearance of low conductivity results at that profile. It is conceivable that the fault is the cause of the low conductivity at this point, since the electrical properties of rocks can change at faults. In this regard it is worth mentioning that this fault runs in northeastern extension over an area which represents a mafic intrusion. This mafic intrusion ends at the mapped surface at the northeast end of profiles 5 and 6. Whether the fault caused the intrusion to reach the surface at this point, or whether the fault formed because an intrusion occurred at this point, cannot be answered with the provided data. Nevertheless, the fault itself has an effect on the VLF-EM results, since VLF-EM is sensitive to differences in conductivity caused by the fault. Although there are no mapped geological phenomena in the vicinity of profiles 1 and 2, large-area anomalies can be detected in three measurements on different days and with different frequencies. Even if in 3 measurements at two different locations similarities can be found in the VLF -EM results, the appearing on 11.02.2019 at 24,0 kHz is radically differing. The results are not to be found in any other profile and it even seems as if the anomalies occur, where the other observations do not show any anomalies at all. In the case that a fault is the cause of the anomaly and the fault is so narrow and additionally falls at an angle that strikes one profile but not the adjacent profile, this characteristic could be justified. In this context, there is actually a fault that runs from north to south and strikes profiles 4 and 5 at such an angle. Since corresponding anomalies can only be seen in this measurement at 24,0 kHz and all other measurements do not show any anomalies, the reason for these results seems to be somewhere else.

Remote Sensing superficial iron anomalies exhibit no particular similarities in blending with geological features and certainly with VLF-EM data. Although minor areas of iron concentrations can be found in region 2 when comparing the more distant surroundings, there are no locally pronounced patterns. However, two distinctive rock samples “b” and “c” were investigated, sample “b” being gossan and sample “c” being quartzite with hematite in fractures and pores within, which should result in increased remote sensed iron concentrations at that location. This is not the case, however, even though theses samples were found directly on profile 4 and directly in a fault zone (figure 8). Even if the remote sensing data does not really match the locations of the rock samples, the following is quite noteworthy. Both rock samples show increased copper concentrations in the range of 0.01 wt.%. A further 2 rocks “d” and “e” with high cobalt concentrations were found between Region 1 and Region 2. Rock “d” is gneiss with 0.018 wt.% cobalt while sample “e” is gossan with approximately 0.015 wt.% cobalt. Consequently, there are also indications of the presence of ores in Region 2 and even beyond Region 2 (see figure 8). A rock sample with significantly increased electrical conductivity due to increased metal content is clear evidence for the presence of these rocks in the subsurface, even more important than the VLF-EM results, because it is a direct result and not an indirect measurement. However, these rocks were not found in the existing bedrock, but as loose pieces. Although it is obvious to claim that they were not very far away from the original source rock, this is certainly not guaranteed. Hence, rock samples are not conclusive evidence of the local occurrence of anomalies, or in other words: It is difficult to determine from the rock samples where exactly further investigation should be carried out. However, they serve very well to support the assumption that there are rocks with significant ore contents in the vicinity of the study area. To make a statement through VLF-EM about the material causing the anomalies is highly speculative and should be avoided. It is a useful method to localize considerable differences in conductivity (Aina & Emofurieta 1991). Again, the presence of rocks with the respective increased concentration of metals can be an important reason for these differences in conductivity, but only the VLF-EM data recorded 11.02.2019 at 24,0 kHz indicate anomalies in the junction of these rock sample locations (figure 10).

6 Conclusions & Summary

As technology advances and the ability to perform ever more complex and comprehensive calculations improves, the VLF-EM method has achieved a kind of renaissance. However, it is still a tedious process to display the VLF-EM results in three-dimensional space, as there is currently no way to quickly process and display the data within a single program. Nevertheless, the data could be blended with geological data, total magnetic intensity surveys and remote sensing of the occurrence of superficial iron anomalies. The results have provided useful indications of areas for future investigation.

- Surveying in Region 1 at coordinates 281950/163000 indicates a subsurface anomaly supported by remote sensing data, a mapped fault and one VLF-EM measurement. However, from VLF-EM prospection this is a rather vague assumption, since it is only confirmed by one of four total measurements. Additionally, the signal strength was weak during this measurement and it shows rather steep and thin appearance of the anomaly.
- Region 2 at coordinates 283250/164300 seems to be interesting for further and more comprehensive investigations. The VLF-EM results with the most reliable signal strengths (how strongly the signal from the antenna can be received at the study area) all point to this area and the dimension of the anomaly is also considerably larger than all other measurements of the whole survey. An already mapped fault also runs through the rocks in this area, but

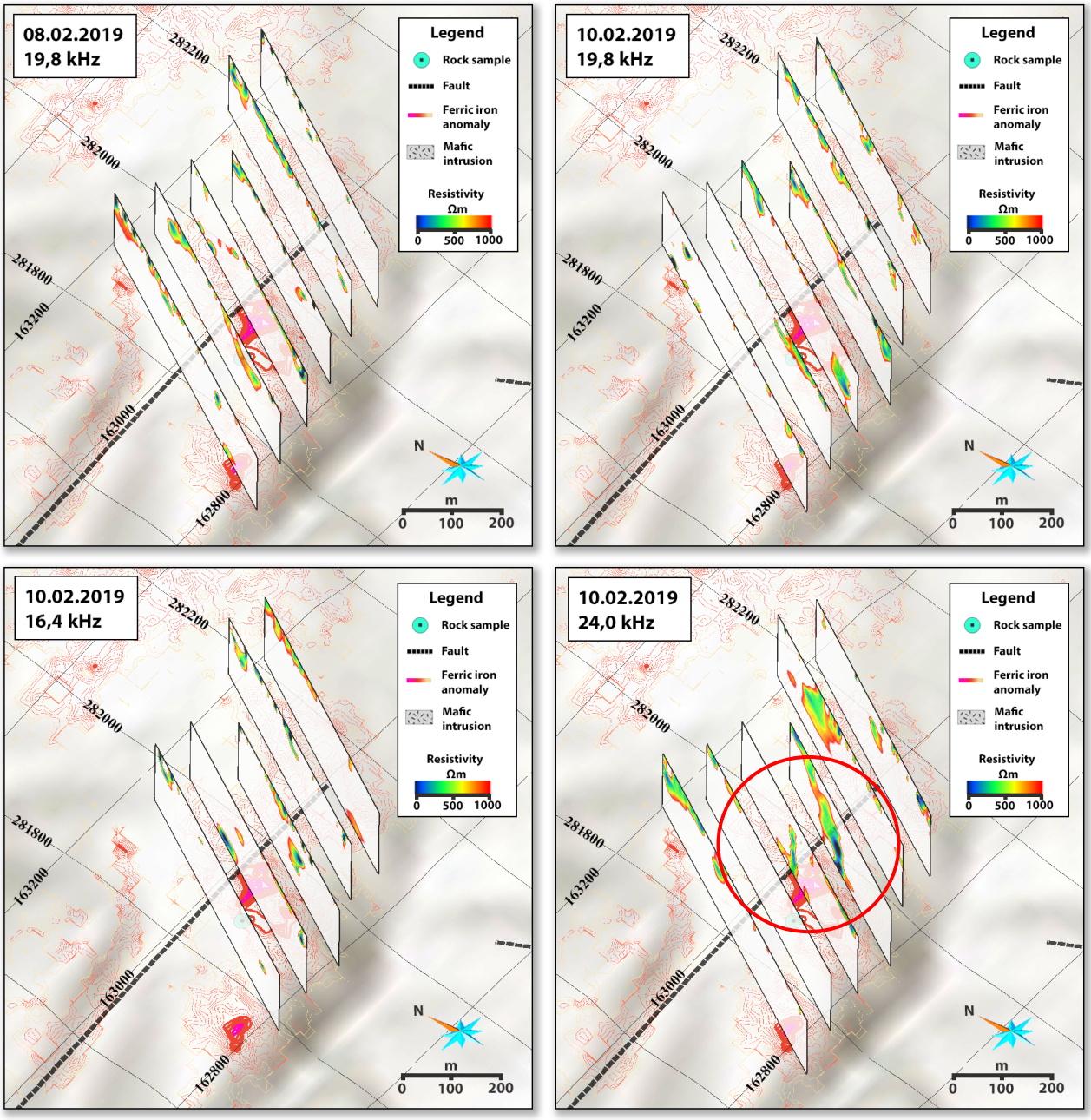

Fig. 9. VLF-EM results of Region 1 blended with geological data and results of remote sensing. Thereby the profiles are always at the same position but measured with different frequencies at different times (see box upper left corner). All profiles lie on a digital elevation model (DEM) of the surface of the terrain, which is displayed in gray scales. An UTM 36N grid with a length of 100 meters per cell is included.The red circle refers to the area of measurement results, which would probably be the most promising place for subsequent investigations and is also the subject of discussion.

there are no striking features revealed by remote sensing data.

The objectives of study were to identify potential electrical conductivity anomalies with the VLF-EM technique and to locally define these anomalous areas where future investigations could be realized. It should be emphasized in this context that VLF-EM is not a method to provide strong evidence for ore rich bedrock alone rather than detect contrasts in electrical conductivity and therefore presenting local anomalous areas. For the purpose of this study, the method is cost -effective for prospecting, but requires blending additional data to make more reliable statements about the subsurface. What the cause for these anomalies is and, rather, what characteristic material in the subsurface the source of the anomaly is, can only be determined ultimately through drilling.

7 Acknowledgements

At this point I would like to express my sincere gratitude to the following persons without whom this work would not have been realized. First of all, I would like to thank my supervisor Dr. Rouwen Lehné, who made

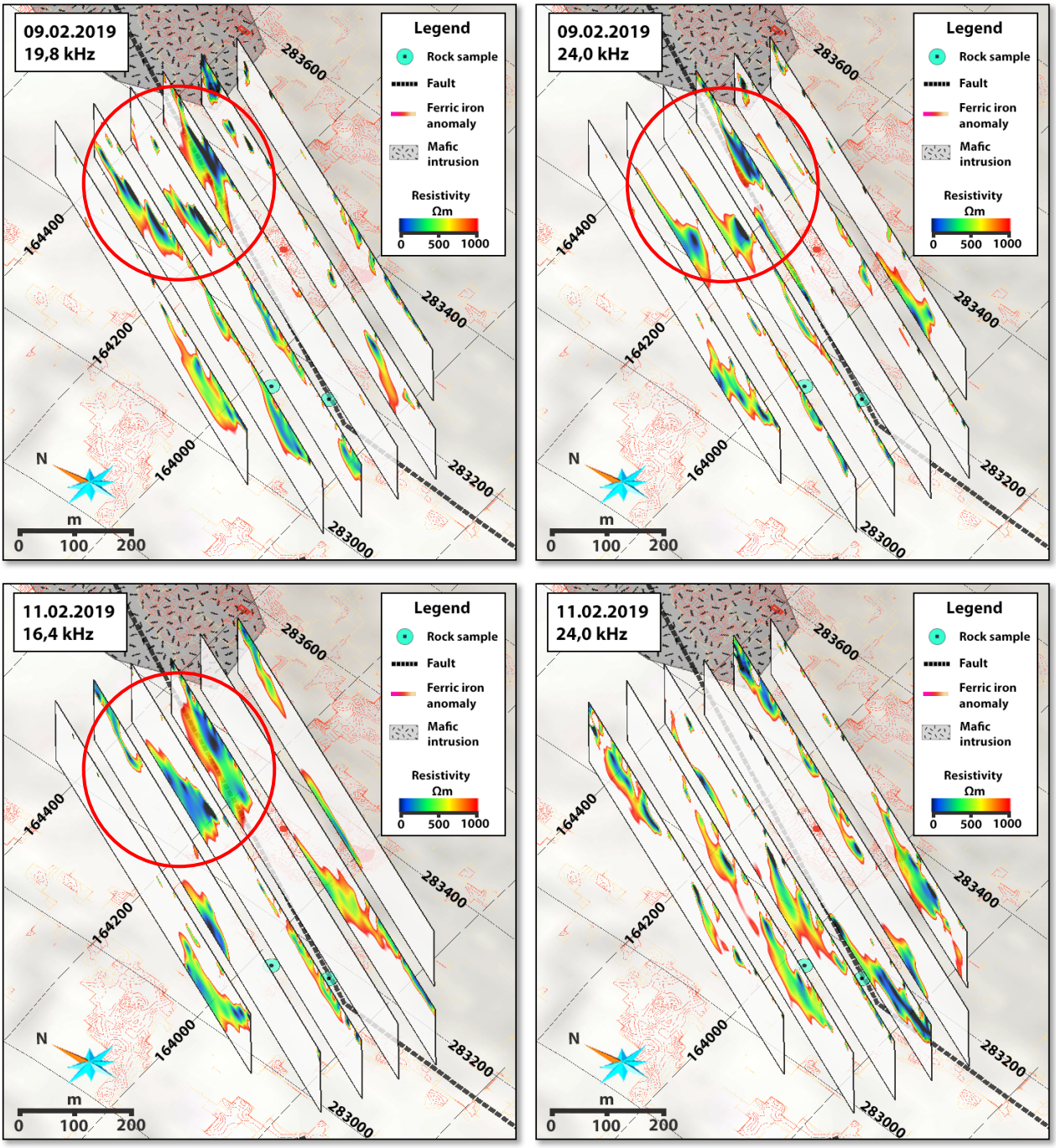

Fig. 10. VLF-EM results of Region 2 blended with geological data and results of remote sensing. Thereby the profiles are always at the same position but measured with different frequencies at different times (see box upper left corner). All profiles lie on a digital elevation model (DEM) of the surface of the terrain, which is displayed in gray scales. An UTM 36N grid with a length of 100 meters per cell is included. The red circles refer to the area of measurement results, which would probably be the most promising place for subsequent investigations and is also the subject of discussion.

the entire cooperation possible in the first place, and all those involved of Rockinol Limited and the Geological Survey in Uganda. I would also like to thank Prof. Dr. Ulf Söderlund for agreeing supervise this work. Furthermore, Prof. Dr. Dan Hammarlund, Henrik Stålhane, Martin Nalepa and Britta Smångs for the organizational assistance and with my questions throughout my entire time in Lund. I would also like to thank Dr. Christoph Butz for his exceptional contribution to the analysis of the raw data and support with the field work in Uganda, M. Sc. Jacob Wächter for his help with the use of Paradigm SKUA-GOCAD program, M.Sc. Eva Loerke for her valuable feedback and of course Dr. Bert Rein for providing high quality remote sensing data.

8 References

Abeinomugisha, D. & Kasande, R., 2013. Tectonic Control on Hydrocarbon Accumulation in the Intracontinental Albertine Graben of the East African Rift System. In: Gao, D. (ed.), *Tec tonics and Sedimentation.* American Associati on of Petroleum Geologists, Tulsa, Oklahoma. 209–228.

Aina, A. & Emofurieta, W.O., 1991. The use of very low frequency electromagnetic method for non-conductive resource evaluation and geological mapping. *Journal of African Earth Sciences (and the Middle East),* 12 (4), 609–616. doi: 10.1016/0899-5362(91)90023-R

AmanigaRuhanga, I. & Manyindo, J., 2010. UGANDA'S ENVIRONMENT AND NATU RAL RESOURCES: ENHANCING PARLIA MENT'S OVERSIGHT.

Basokur, A.T. & Candansayar, M.E., 2003. Enhan cing VLF data for qualitative interpretation: An example of massive chalcopyrite exploration. *The Leading Edge*, 22 (6), 568–570. doi: 10.1190/1.1587680

Butz, C., Lehné, R. & Rein, B., 2018. Report on the field campaign undertaken in the Hoima region (Uganda) – concession area EL1274 in August 2018.

Chorowicz, J., 2005. The East African rift system. *Journal of African Earth Sciences*, 43 (1-3), 379 –410. doi: 10.1016/ j.jafrearsci.2005.07.019

Delvaux, D. & Barth, A., 2010. African stress pattern from formal inversion of focal mechanism data. *Tectonophysics*, 482 (1-4), 105–128. doi: 10.1016/j.tecto.2009.05.009

Dentith, M.C. & Mudge, S.T., 2014. Geophysics for the mineral exploration geoscientist. Cambridge University Press, Cambridge.

Ebinger, C.J., 1989. Tectonic development of the western branch of the East African rift system. *Geological Society of America Bulletin*, 101 (7), 885–903. doi: 10.1130/0016-7606(1989) 101<0885:TDOTWB>2.3.CO;2

Fraser, D.C., 1969. Contouring of VLF-EM data. *GE OPHYSICS*, 34 (6), 958–967. doi: 10.1190/1.1440065

GEM Systems, I., 2008. GSM-19 v7.0 Instruction Ma nual: Manual Release 7.4, Markham, Canada.

GTK CONSORTIUM, 2011. SUSTAINABLE MA NAGEMENT OF MINERAL RESOURCES PROJECT: GEOLOGICAL MAPPING, GEO CHEMICAL SURVEYS AND MINERAL RESOURCES ASSESSMENT IN SELECTED AREAS OF UGANDA: Contract No.: MEMD/ SMMRP/services/2006/00004 NDF. GTK CONSORTIUM.

Isabirye, E., 2008. Core logging of two (2) drill holes at Kabaale - Buseruka, Hoima District - A short report.

KAMPUNZU, A.B., AKANYANG, P., MAPEO, R.B.M., MODIE, B.N. and WENDORFF, M., 1998. Geochemistry and tectonic significance of the Mesoproterozoic Kgwebe metavolcanic rocks in northwest Botswana: implications for the evolution of the Kibaran Namaqua-Natal Belt. *Geological Magazine*, 135 (5), 669–683. doi: 10.1017/S001675689800123X

Karous, M. & Hjelt, S.E., 1983. Linear filtering of VLF dip angle measurements.*. *Geophysical Prospecting,* 31 (5), 782–794. doi: 10.1111/ j.1365-2478.1983.tb01085.x

Karp, T., Scholz, C.A. & McGlue, M.M., 2012. Structure and Stratigraphy of the Lake Albert Rift, East Africa: Observations from Seismic Reflection and Gravity Data. In: O.W. Baganz, Y. Bartov, K. Bohacs, D. Nummedal (ed.), *La custrine Sandstone Reservoirs and Hydrocar bon Systems:* AAPG Memoir 95. 299–318.

Kearey, P., Brooks, M. & Hill, I., 2001. An introduc tion to geophysical exploration. 3rd ed. Black well Science, Malden, MA.

Knödel, K. (ed.), 2005. Geophysik: Mit 57 Tabellen. Handbuch zur Erkundung des Untergrundes von Deponien und Altlasten, Bd. 3. 2nd ed. Springer, Berlin, Heidelberg, New York. XXXII, 1102 Seiten.

Mallet, J.-L., 1989. Discrete smooth interpolation. ACM Transactions on Graphics, 8 (2), 121–144. doi: 10.1145/62054.62057

McNeill, J.D. & Labson, V.F., 1991. 7. Geological Mapping Using VLF Radio Fields. In: Nabighi an, M.N. (ed.), Electromagnetic Methods in *Applied Geophysics. Society of Exploration Geophysicists.* 521–640.

Ministry of Energy and Mineral Development Uganda, 2018. MINING AND MINERAL POLICY FOR UGANDA 2018. Irene Muloni.

Monteiro Santos, F.A., Mateus, A., Figueiras, J. & Gonçalves, M.A., 2006. Mapping groundwater contamination around a landfill facility using the VLF-EM method — A case study. *Journal of Applied Geophysics,* 60 (2), 115–125. doi: 10.1016/j.jappgeo.2006.01.002

Morley, C.K., 1989. Extension, detachments, and sedi mentation in continental rifts (with particular reference to East Africa). *Tectonics*, 8 (6), 1175 –1192. doi: 10.1029/tc008i006p01175

Nyblade, A.A. & Langston, C.A., 1995. East African earthquakes below 20 km depth and their impli cations for crustal structure. *Geophysical Jour nal International,* 121 (1), 49–62. doi: 10.1111/ j.1365-246X.1995.tb03510.x

Owuor, S., 2019. What Are The Major Natural Re sources Of Uganda?: https:// www.worldatlas.com/articles/what-are-the-major-natural-resources-of-uganda.html. Acces sed September 27, 2019.

Paál, G., 1965. Ore prospecting based on VLF-radio signals. *Geoexploration*, 3 (3), 139–147. doi:

10.1016/0016-7142(65)90016-5
Pedersen, L.B., Persson, L., Bastani, M. & Byström, S., 2009. Airborne VLF measurements and mapping of ground conductivity in Sweden. *Journal of Applied Geophysics*, 67 (3), 250–258. doi: 10.1016/j.jappgeo.2007.11.002
Prodehl, C., Fuchs, K. & Mechie, J., 1997. Seismic-refraction studies of the Afro-Arabian rift sys tem — a brief review. *Tectonophysics*, 278 (1-4), 1–13. doi: 10.1016/S0040-1951(97)00091-7
Reynolds, J.M., 2011. An introduction to applied and environmental geophysics. 2nd ed. Wiley-Blackwell, Chichester. 696 p. [In eng]
Richardson, R.M., 1992. Ridge forces, absolute plate motions, and the intraplate stress field. *Journal of Geophysical Research*, 97 (B8), 11739. doi: 10.1029/91jb00475
Rosendahl, B.R., 1987. Architecture of Continental Rifts with Special Reference to East Africa. *Annual Review of Earth and Planetary Sci ences*, 15 (1), 445–503. doi: 10.1146/ an nurev.ea.15.050187.002305
Sasaki, Y., 1989. Two-dimensional joint inversion of magnetotelluric and dipole-dipole resistivity data. *GEOPHYSICS*, 54 (2), 254–262. doi: 10.1190/1.1442649
Saydam, A.S., 1981. Very-low-frequency electromag netic interpretation using tilt angle and elliptici ty measurements. *GEOPHYSICS*, 46 (11), 1594–1605. doi: 10.1190/1.1441166
Simiyu, S.M. & Keller, G.R., 1997. An integrated analysis of lithospheric structure across the East African plateau based on gravity anomalies and recent seismic studies. *Tectonophysics*, 278 (1-4), 291–313. doi: 10.1016/S0040-1951(97) 00109-1
Strecker, M.R., Blisniuk, P.M. & Eisbacher, G.H., 1990. Rotation of extension direction in the central Kenya Rift. *Geology*, 18 (4), 299. doi: 10.1130/0091-7613(1990) 018<0299:ROEDIT>2.3.CO;2
Upcott, N.M., Mukasa, R.K., EBINGER, C.J. & Kar ner, G.D., 1996. Along-axis segmentation and isostasy in the Western rift, East Africa. *Jour nal of Geophysical Research*, 101 (B2), 3247– 3268. doi: 10.1029/95JB01480
Zoback, M.L., 1992. First- and second-order patterns of stress in the lithosphere: The World Stress Map Project. *Journal of Geophysical Research*, 97 (B8), 11703. doi: 10.1029/92JB00132

APPENDIX I

Explanation of the physical background behind VLF-EM

The underlying principle of the Very-Low-Frequency Electromagnetic (VLF-EM) method is based on electromagnetism, more precisely the interaction between electric currents and magnetism. The basis of electromagnetism lies in the Maxwell equations and their underlying principle. For this work and for understanding the VLF-EM method the reflections of James Clerk Maxwell from the 1860s, known as Maxwell equations, are essential. These equations describe the behavior of electric and magnetic fields, but their deduction is mathematically very complex. Therefore, these equations are here only explained briefly. For a detailed discussion of the Maxwell equations including derivation for the application of VLF-EM methods in geoscientific problems, refer to the work of (McNeill and Labson 1991). The first Maxwell equation is called Gauss's law and states in principle that the electric field has a source in form of charges. This electric charge can be positive or negative. The second Maxwell equation is called Gauss's law for magnetism and states the magnetic field has no source. While electric charges can be separated to create an electric field between them, this is not possible for magnetic fields. According to present-day state of knowledge, there are no magnetic monopoles. The third Maxwell equation states that a time-varying magnetic field induces an electric field and is known as Faraday's law of induction. In the other direction is the fourth Maxwell equation, which states that a temporally changing electric field induces a magnetic field. This equation is also called Ampere's law.

The last two equations yield the core essence of the Very-Low-Frequency-Electromagnetic (VLF-EM) methodology: The connection of electric and magnetic fields is coupled to each other and induce one another. This coupling is utilized by the VLF-EM method and provides information about the characteristics of the subsurface. Electric fields are created by the basic structure of atoms with positively charged protons in the atomic nucleus and negative free electrons in the surrounding atomic shells. Charges always have an electric field and between different charges the respective fields affect each other in space and generate a force according to Coulomb's law such as the same charges will repel each other and attract if they are of opposite charge. Due to the mobility of electrons, these charges can move from one place to another if, for example, it is a material that provides a particularly large number of electrons with high mobility, as is the case for metals. Therefore, metals are often called electrical conductors, whereas materials in which electrons are less freely mobile are called non-conductors or insulators. This point is important because the VLF-EM method is intended to visualize these differences in the mobility of electrons between rocks. The term used to describe this is electrical conductivity. The higher the mobility of electrons, the higher the electrical conductivity of the medium. Since rocks are generally poor electrical conductors, the term electrical resistivity is more commonly applied. The electrical resistivity is simply the reciprocal of the electrical conductivity.

Besides, charges in insulators can also be made "visible" by rubbing a cloth against a glass stick, for example, and then "rubbing" electrons from one insulator to another, or transferring electrons from one object to another, thus creating a charge difference. This can be recognized by the fact that the charged object exerts a force on neutral materials and, for example, pulls hairs on the actual non-conductive glass rod. Since a charge difference has been created by friction and the charges cannot "flow off" freely in an insulator, the effect of that force can actually be readily observed. Although this effect makes charges seemingly continuous, the charges are actually quantized. This means that as an electron has a charge $e = 1.602 \cdot 10{-}19$ Coulomb (elementary charge), an object can only emit or absorb multiples of this elementary charge. Since this elementary charge is so small, it is not noticeable macroscopically. When electrons are in motion, so are charges. Moving charges are called electric current. It should be noted that there are historically two current directions, since it was originally assumed that the positively charged particles could move and generate a current. This movement of the positively charged particles is therefore also called "technical" current direction and it marks the direction from positive to negative (also called from north to south). The "real" or "physical" current direction, on the other hand, describes the actual movement of the electrons from negative to positive (south to north), as in fact only the negatively charged electrons are actually moving. For VLF-EM measurements, this relationship is crucial and is a prerequisite when doing field measurements. Even if the VLF device processes the measurements in such a way that one does not have to bother about whether the real or the technical current direction is determined, one should always keep an overall picture of all variables and especially their current directions. For this reason, it needs to be emphasized at this point that the technical flow direction is generally addressed throughout the work.

It also makes a difference in which direction the entire measuring profiles are recorded and whether this direction of the measuring profiles is also reasonably aligned. It is emphasized briefly once again why this should not be done arbitrarily: The components of the magnetic and electric field are vectors and because of that they are parameters with a given angle to each other, to the earth's surface, to the transmitter and to the investigated anomaly in the underground. The direction from which the transmitted signal comes from the antenna is fixed, but different signals can be induced by different positions of the anomaly in the ground, depending on the direction in which direction

the measurements are carried out on the surface. The vector separation of these signals is also described in the VLF-EM method, but it deserves to be noted at this point that even an ore-rich path (excellent electrical conductor) may not be localized only because an inappropriate direction of measurement has been adopted.

Once an electric current flows a magnetic field is generated. At the instant the magnetic field is changed, a current is induced in an interspersed conductor within this magnetic field, which is referred to as induction. According to Lenz's law, this current always opposes its source. So, a change of the electric field influences the magnetic field and vice versa. Therefore, it is referred to as an electromagnetic field. The force which acts in an electromagnetic field is called Lorentz force and is perpendicular to the direction of movement of the charge as well as to the direction of the magnetic field. Electricity and magnetism or electric currents and magnetic fields are therefore inseparably connected, since the source of the electric field is always a charge and magnetic fields are created by the movement of this charge, which are however free of any source themselves. The causality of moving charges and the resulting magnetism is separate from materials that have a magnetic field (such as a permanent magnet), even if there are no apparent moving charges.

Although most people know the functional principle of a permanent magnet, the reason for this magnetism cannot be explained without further effort. This requires the special theory of relativity and quantum mechanics, since charges are also present in the structure of matter. In this context only a very brief outline is given of how this basic principle of quantum mechanics works. The protons and electrons of the atoms involved behave as if they rotated around an axis, which is called magnetic moment or spin. Thus, magnetism is inevitably linked to motion, whether through the motion of numerous charges or the self-rotation of the individual particles of matter. Depending on how these particles are aligned in a material, different types of magnetism are generated. In general, a distinction is made between ferromagnetism, diamagnetism and paramagnetism. With ferromagnetism, numerous particles remain ordered in so-called magnetic domains and ferromagnetism means that the spin of particles is aligned in the same way. In diamagnetism, this frequent redirection of the spin cannot be produced, and paramagnetism means, an external magnetic field can cause alignment to a certain degree.

An electromagnetic wave is the spatial and temporal propagation of the coupled electric and magnetic fields in the form of a wave at the speed of light. No matter, but only energy is transported through a medium or even through a vacuum. The electromagnetic wave is a transverse wave with the components of the electric and magnetic field perpendicular to both each other and the direction of propagation of the wave (refer figure 3 and figure 11). There is a large spectrum of electromagnetic waves and VLF waves can be found at the end of the spectrum characterized by having with low frequency and large wavelengths (figure 2). It is known from quantum mechanics that matters have both wave and particle properties. While wave properties dominate in the low frequency range of VLF and also in the radio range, particle properties at the other end of the electromagnetic spectrum predominate in the X-ray and gamma radiation range. The wave properties of the electromagnetic wave include reflection, refraction, diffraction and interference, which play an important role in the use of the VLF-EM methodology as they significantly influence the resulting data properties.

When performing VLF-EM measurements, an antenna is used for generating an electromagnetic wave. Inside the antenna electric current continuously change the direction along the antenna due to an applied alternating voltage. The alternating voltage causes charges to move periodically in the antenna, which can be described mathematically as a sinusoidal curve with a certain wavelength and frequency. Furthermore, a magnetic field perpendicular to the antenna is generated by these moving charges, which then also "resonates" with the electric wave. The result is an electromagnetic wave with a vertical oscillating electrical component and a horizontal oscillating magnetic component, which propagates radially from the transmitting antenna.

The primary electromagnetic wave with the horizontal magnetic and vertical electrical components then encounters the electrically conductive body, which provides free electrons to move within that body inducing a voltage in it. According to Faraday's law of induction the induced voltage depends on the change in the magnetic field, which means that the induced voltage lags behind the primary magnetic component

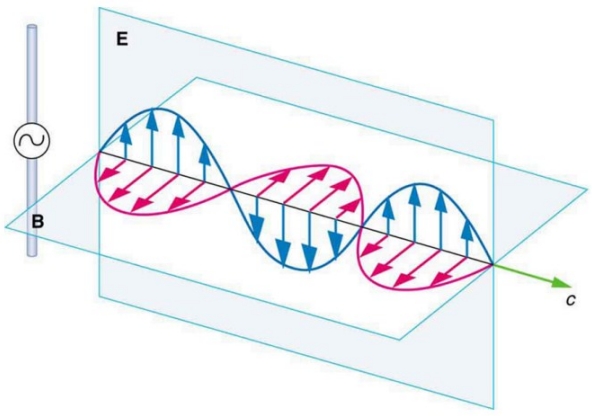

Fig. 11. The electromagnetic wave propagates perpendicularly from the transmitting antenna at light speed c. The electrical component E and the magnetic component B are perpendicular to each other. The electric field of a vertical antenna also moves vertically, while the magnetic field moves horizontally in the propagation direction (edited after Gitman *et al*. (2017)).

by 90° (π/2), because it takes a finite time to generate this voltage. In other words, when the wave of the primary magnetic field reaches its maximum or minimum, the induced voltage in the body is zero. As a result, the primary wave and the indicated voltage in the body are out of phase by 90°. The induced voltage in the body causes eddy currents within the body, which take some time to flow. The delay is simply an additional phase lag between the induced voltage and the induced current. This phase shift depends on the electrical properties of the body and is large when the body is conductive and small when the body is poorly conductive. The moving charges in the form of eddy currents form a secondary magnetic field, which surrounds the body. It depends on the strength of the primary magnetic field, the attenuation by the underground and above all the electrical characteristics of the body itself.

APPENDIX II

Disassembly of magnetic field vectors

As both magnetic fields (primary horizontal and secondary vertical) interfere with each other, a resulting magnetic field is generated with a resulting phase shift in relation to the original wave of the primary field. By comparing the primary signal with the resulting signal, it is possible to describe the subsurface condition. The following procedure is designed to illustrate the process of determining these variables based on Kearey *et al*. (2001). Figure 12 provides a visual outline of the following steps and describes the respective components of the primary and secondary signal.

1. The primary magnetic field P propagates in the form of a sine wave. The amplitude of this wave indicates the magnitude of the vector P. A vector diagram is used to illustrate the different magnetic fields. The first vector P represents the primary magnetic field at the point of measurement, i.e. the signal emitted by the transmitter.
2. If the wave of the primary magnetic field P hits an electrically conductive body in the underground, a voltage is induced by electromagnetic induction. This voltage is shifted by 90° (π / 2) to the primary magnetic field (Faraday's law). The corresponding vector Sy of the induced voltage is plotted perpendicularly to the primary field vector P. This vector is then plotted against the primary field vector (P). It is called imaginary part or out-of-phase part.
3. The induced voltage produces electric eddy currents and this current is additionally phase-shifted by α. The reason for this is the time required to let this electric current flow in the electrically conductive body and is therefore directly dependent on its electrical conductivity. In order to represent the additional phase shift α, the vector S is ablated by an angle α starting from the vector Sy and describes the secondary induced magnetic field S. The larger the angle α, the better the electrical conductivity of the body.
4. The secondary magnetic field S and the primary magnetic field P overlap each other and form the resulting magnetic field R. This magnetic field R differs from the primary magnetic field P in strength (amplitude) and also in phase. This phase shift is marked with φ. The secondary magnetic field S can be calculated by vector decomposition into imaginary or out-of-phase part (Sy) and real or in-phase part (Sx) and finally gives information about the electrical properties of the subsurface at the measuring point. The larger the real or in-phase part (Sx) compared to the imaginary or out-of-phase part (Sy), the better the electrical conductivity.

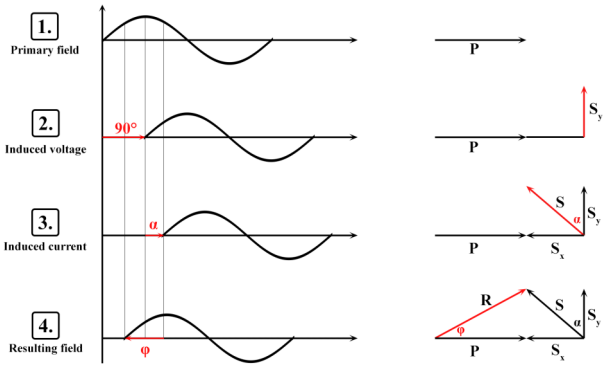

Fig. 12. Illustration of the phase lags using sine curves and vector decomposition to calculate the utilized parameters. The phase lag of the primary signal of the electromagnetic wave of the antenna (1.) to the induced voltage in an electrically conductive body in the underground (2.) is 90° initially. The current which then flows in this body continues to be phase-lagged depending on its electrical properties (3.). This results in a resulting phase lag (4.) to be measured in the field and thus necessitates decomposition into vectors. A detailed description of the individual points can be found in the text (based on Kearey *et al*. 2001)

Tidigare skrifter i serien ”Examensarbeten i Geologi vid Lunds universitet”:

525. Becker Jensen, Amanda, 2017: Den eocena Furformationen i Danmark: exceptionella bevaringstillstånd har bidragit till att djurs mjukdelar fossiliserats.(15 hp)
526. Radomski, Jan, 2018: Carbonate sedimentology and carbon isotope stratigraphy of the Tallbacken-1 core, early Wenlock Slite Group, Gotland, Sweden. (45 hp)
527. Pettersson, Johan, 2018: Ultrastructure and biomolecular composition of sea turtle epidermal remains from the Campanian (Upper Cretaceous) North Sulphur River of Texas. (45 hp)
528. Jansson, Robin, 2018: Multidisciplinary perspective on a natural attenuation zone in a PCE contaminated aquifer. (45 hp)
529. Larsson, Alfred, 2018: Rb-Sr sphalerite data and implications for the source and timing of Pb-Zn deposits at the Caledonian margin in Sweden. (45 hp)
530. Balija, Fisnik, 2018: Stratigraphy and pyrite geochemistry of the Lower–Upper Ordovician in the Lerhamn and Fågelsång -3 drill cores, Scania, Sweden. (45 hp)
531. Höglund, Nikolas, 2018: Groundwater chemistry evaluation and a GIS-based approach for determining groundwater potential in Mörbylånga, Sweden. (45 hp)
532. Haag, Vendela, 2018: Studie av mikrostrukturer i karbonatslagkäglor från nedslagsstrukturen Charlevoix, Kanada. (15 hp)
533. Hebrard, Benoit, 2018: Antropocen – vad, när och hur? (15 hp)
534. Jancsak, Nathalie, 2018: Åtgärder mot kusterosion i Skåne, samt en fallstudie av erosionsskydden i Löderup, Ystad kommun. (15 hp)
535. Zachén, Gabriel, 2018: Mesosideriter – redogörelse av bildningsprocesser samt SEM-analys av Vaca Muertameteoriten. (15 hp)
536. Fägersten, Andreas, 2018: Lateral variability in the quantification of calcareous nannofossils in the Upper Triassic, Austria. (15 hp)
537. Hjertman, Anna, 2018: Förutsättningar för djupinfiltration av ytvatten från Ivösjön till Kristianstadbassängen. (15 hp)
538. Lagerstam, Clarence, 2018: Varför svalde svanödlor (Reptilia, Plesiosauria) stenar? (15 hp)
539. Pilser, Hannes, 2018: Mg/Ca i bottenlevande foraminiferer, särskilt med avseende på temperaturer nära 0°C. (15 hp)
540. Christiansen, Emma, 2018: Mikroplast på och i havsbotten - Utbredningen av mikroplaster i marina bottensediment och dess påverkan på marina miljöer. (15 hp)
541. Staahlnacke, Simon, 2018: En sammanställning av norra Skånes prekambriska berggrund. (15 hp)
542. Martell, Josefin, 2018: Shock metamorphic features in zircon grains from the Mien impact structure - clues to conditions during impact. (45 hp)
543. Chitindingu, Tawonga, 2018: Petrological characterization of the Cambrian sandstone reservoirs in the Baltic Basin, Sweden. (45 hp)
544. Chonewicz, Julia, 2018: Dimensionerande vattenförbrukning och alternativa vattenkvaliteter. (15 hp)
545. Adeen, Lina, 2018: Hur lämpliga är de geofysiska metoderna resistivitet och IP för kartläggning av PFOS? (15 hp)
546. Nilsson Brunlid, Anette, 2018: Impact of southern Baltic sea-level changes on landscape development in the Verkeån River valley at Haväng, southern Sweden, during the early and mid Holocene. (45 hp)
547. Perälä, Jesper, 2018: Dynamic Recrystallization in the Sveconorwegian Frontal Wedge, Småland, southern Sweden. (45 hp)
548. Artursson, Christopher, 2018: Stratigraphy, sedimentology and geophysical assessment of the early Silurian Halla and Klinteberg formations, Altajme core, Gotland, Sweden. (45 hp)
549. Kempengren, Henrik, 2018: Att välja den mest hållbara efterbehandlingsmetoden vid sanering: Applicering av beslutsstödsverktyget SAMLA. (45 hp)
550. Andreasson, Dagnija, 2018: Assessment of using liquidity index for the approximation of undrained shear strength of clay tills in Scania. (45 hp)
551. Ahrenstedt, Viktor, 2018: The Neoproterozoic Visingsö Group of southern Sweden: Lithology, sequence stratigraphy and provenance of the Middle Formation. (45 hp)
552. Berglund, Marie, 2018: Basaltkuppen - ett spel om mineralogi och petrologi. (15 hp)
553. Hernnäs, Tove, 2018: Garnet amphibolite in the internal Eastern Segment, Sveconorwegian Province: monitors of metamorphic recrystallization at high temperature and pressure during Sveconorwegian orogeny. (45 hp)
554. Halling, Jenny, 2019: Characterization of black rust in reinforced concrete structures: analyses of field samples from southern Sweden. (45 hp)
555. Stevic, Marijana, 2019: Stratigraphy and

dating of a lake sediment record from Lyngsjön, eastern Scania - human impact and aeolian sand deposition during the last millennium. (45 hp)

556. Rabanser, Monika, 2019: Processes of Lateral Moraine Formation at a Debris-covered Glacier, Suldenferner (Vedretta di Solda), Italy. (45 hp)
557. Nilsson, Hanna, 2019: Records of environmental change and sedimentation processes over the last century in a Baltic coastal inlet. (45 hp)
558. Ingered, Mimmi, 2019: Zircon U-Pb constraints on the timing of Sveconorwegian migmatite formation in the Western and Median Segments of the Idefjorden terrane, SW Sweden. (45 hp)
559. Hjorth, Ingeborg, 2019: Paleomagnetisk undersökning av vulkanen Rangitoto, Nya Zeeland, för att bestämma dess utbrottshistoria. (15 hp)
560. Westberg, Märta, 2019: Enigmatic worm-like fossils from the Silurian Waukesha Lagerstätte, Wisconsin, USA. (15 hp)
561. Björn, Julia, 2019: Undersökning av påverkan på hydraulisk konduktivitet i förorenat område efter in situ-saneringsförsök. (15 hp)
562. Faraj, Haider, 2019: Tolkning av georadarprofiler över grundvattenmagasinet Verveln - Gullringen i Kalmar län. (15 hp)
563. Bjermo, Tim, 2019: Eoliska avlagringar och vindriktningar under holocen i och kring Store Mosse, södra Sverige. (15 hp)
564. Langkjaer, Henrik, 2019: Analys av Östergötlands kommande grundvattenresurser ur ett klimtperspektiv - med fokus på förstärkt grundvattenbildning. (15 hp)
565. Johansson, Marcus, 2019: Hur öppet var landskapet i södra Sverige under Atlantisk tid? (15 hp)
566. Molin, Emmy, 2019: Litologi, sedimentologi och kolisotopstratigrafi över krita–paleogen-gränsintervallet i borrningen Limhamn-2018. (15 hp)
567. Schroeder, Mimmi, 2019: The history of European hemp cultivation. (15 hp)
568. Damber, Maja, 2019: Granens invandring i sydvästa Sverige, belyst genom pollenanalys från Skottenesjön. (15 hp)
569. Lundgren Sassner, Lykke, 2019: Strandmorfologi, stranderosion och stranddeposition, med en fallstudie på Tylösand sandstrand, Halland. (15 hp)
570. Greiff, Johannes, 2019: Mesozoiska konglomerat och Skånes tektoniska utveckling. (15 hp)
571. Persson, Eric, 2019: An Enigmatic Cerapodian Dentary from the Cretaceous of southern Sweden. (15 hp)
572. Aldenius, Erik, 2019: Subsurface characterization of the Lund Sandstone – 3D model of the sandstone reservoir and evaluation of the geoenergy storage potential, SW Skåne, South Sweden. (45 hp)
573. Juliusson, Oscar, 2019: Impacts of subglacial processes on underlying bedrock. (15 hp)
574. Sartell, Anna, 2019: Metamorphic paragenesis and P-T conditions in garnet amphibolite from the Median Segment of the Idefjorden Terrane, Lilla Edet. (15 hp)
575. Végvári, Fanni, 2019: Vulkanisk inverkan på klimatet och atmorsfärcirkulationen: En litterarurstudie som jämför vulkanism på låg respektive hög latitud. (15 hp)
576. Gustafsson, Jon, 2019: Petrology of platinum-group element mineralization in the Koillismaa intrusion, Finland. (45 hp)
577. Wahlquist, Per, 2019: Undersökning av mindre förkastningar för vattenuttag i sedimentärt berg kring Kingelstad och Tjutebro. (15 hp)
578. Gaitan Valencia, Camilo Esteban, 2019: Unravelling the timing and distribution of Paleoproterozoic dyke swarms in the eastern Kaapvaal Craton, South Africa. (45 hp)
579. Eggert, David, 2019: Using Very-Low-Frequency Electromagnetics (VLF-EM) for geophysical exploration at the Albertine Graben, Uganda - A new CAD approach for 3D data blending. (45 hp)

LUNDS UNIVERSITET

Geologiska institutionen
Lunds universitet
Sölvegatan 12, 223 62 Lund